An Updated High Precision Measurement of the Neutral Pion Lifetime via the Primakoff Effect

December 10, 2007

THIS ALL NEEDS TO BE UPDATED

Brazilians, new Kharkov people, Bitao

A. Ahmidouch, S. Danagoulian (spokesperson),
A. Gasparian (spokesperson and contact person), C. Jackson, S. Mtingwa, J. Underwood
North Carolina A&T State University, Greensboro, NC

E. Clinton, R. Hicks, D. Lawrence, R. Miskimen (spokesperson)
University of Massachusetts, Amherst, MA

D. Dale (spokesperson), M. Gabrielyan, B. Hu, W. Korsch, A. Teymurazyan, P. Zolnierczuk
University of Kentucky, Lexington, KY

A. Afanasev, E. Chudakoff, H. Egiyan, R. Ent, V. Gyurjyan, M. Ito, J.P. Chen,
Y. Sharabian, E. Smith
Thomas Jefferson National Accelerator Facility, Newport News, VA

K. Baker, M. Christy, J. Goity, P. Gueye, C. Keppel, L. Tang, L. Yuan
Hampton University, Hampton, VA

L. Gan, M. Alexanian, T. Black
University of North Carolina at Wilmington, Wilmington, NC

A.M. Bernstein, D. Hasell, S. Kowalski, R. Suleiman
Massachusetts Institute of Technology, Cambridge, MA

D. Sober, H. Crannell, R. Hakobyan
The Catholic University of America, Washington, DC

J. Ball, M. Dugger, E. Pasyuk, B.G. Ritchie
Arizona State University, Tempe, AZ

R. Minehart, B. Stevens
University of Virginia, Charlottesville, VA

A. Asratyan, O. Chernyshov, G. Davidenko, A. Dolgolenko, G. Dzyubenko, A. Evdokimov,
V. Goryachev, A. Kamenskii, M. Kubantsev, I. Larin, V. Matveev, V. Semyachkin,
A. Sitnikov, V. Verebryusov, V. Vishnyakov

Institute for Theoretical and Experimental Physics, Moscow, Russia

Yu. Goncharenko, V. Kubarovsky, A. Meschanin, L. Soloviev, A. Vasiliev
Institute for High Energy Physics, Protvino, Russia

M. Khandaker, V. Punjabi, C. Salgado
Norfolk State University, Norfolk, VA

A. Glamazdin, A. Omelaenko, ++++++++
Kharkov Institute of Physics and Technology, Kharkov, Ukraine

P.L. Cole
University of Texas at El Paso, El Paso, TX

A. Nathan
University of Illinois, Urbana, IL

C. Li, Z. Liu, S. Lu, J. Yuan, J. Zhou, S. Zhou, X. Zhu
Chinese Institute of Atomic Energy, Beijing, China

J. He
Institute of High Energy Physics, Chinese Academy of Sciences, Beijing, China

W. Briscoe
George Washington University, Washington, DC

I. Aznauryan, S. Gevorgyan, A. Margaryan, K. Egiyan,
H. Voskanyan, A. Ketikyan, A. Shahinyan, A. Petrosyan
Yerevan Physics Institute, Yerevan, Armenia

B. Milbrath
Eastern Kentucky University, Richmond, KY

A.I. Fix, V.A. Tryasuchev
Tomsk Polytechnical University, Tomsk, Russia

M. Elaasar
Southern University at New Orleans, New Orleans, LA

Contents

Abstract

The PrimEx Collaboration has proposed to perform a precision measurement on the two photon decay width of the neutral pion ($\Gamma_{\pi^0\to\gamma\gamma}$). This measurement will provide a stringent test of the predictions of the U(1) axial anomaly in quantum chromodynamics. The first experimental data set was collected in 2004. The new level of experimental precision has been achieved by implementing a high intensity and high resolution photon tagging facility in Hall B at Jefferson Lab and by developing and constructing a state-of-the-art, high resolution electromagnetic calorimeter. A preliminary result on the π^0 lifetime with a precision of $\sim 3\%$ from our first run was released at the American Physical Society April meeting in 2007 through an invited presentation and at American Institute of Physics press conference. Here, we discuss the analysis status on the existing data and the improvement can be made with a future run, and thereby request an extension of the π^0 lifetime measurement from PAC 33 to reach the ultimate goal of $\simeq 1.4\%$ accuracy.

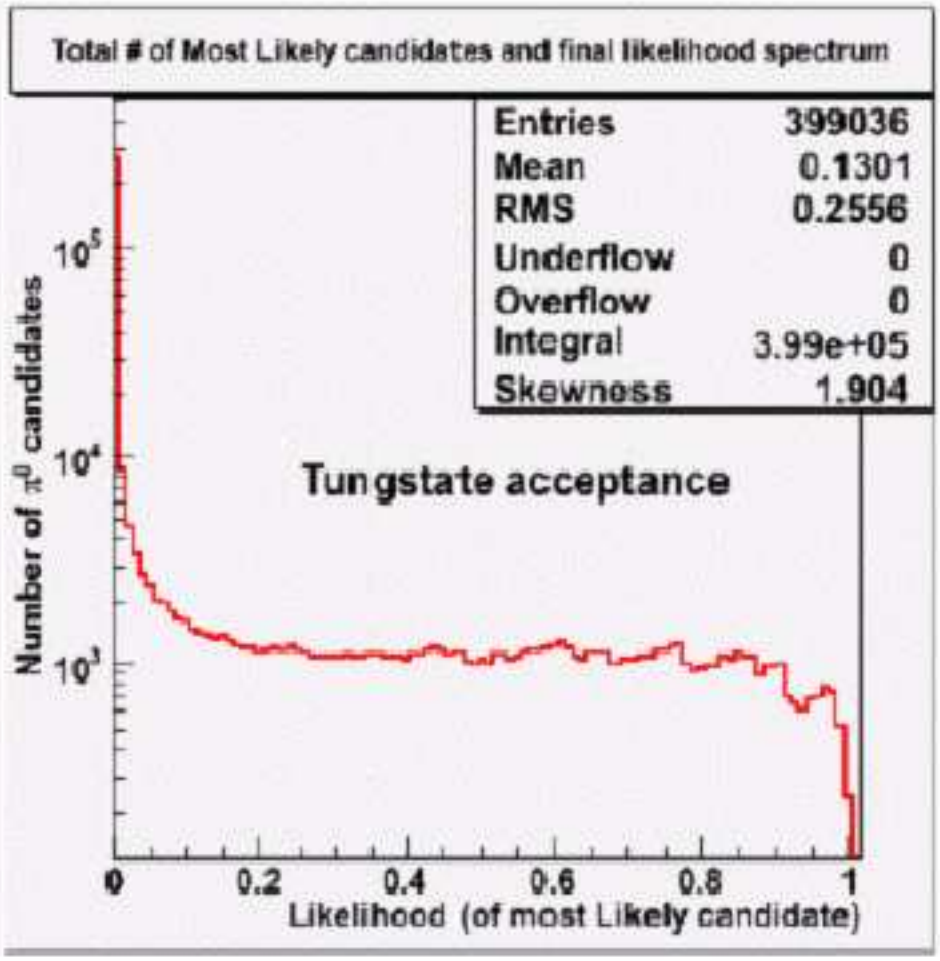

Figure 1: .

1 Motivation

2 Neutral Pion Photoproduction via the Primakoff Effect

3 Theoretical Developments

4 Preliminary Results on the π^o Lifetime

4.1 Cross Section Extraction

4.2 Determination of $\Gamma_{\pi^o \to \gamma\gamma}$

4.3 Theoretical Calculations on Nuclear Forn Factors and Backgrounds

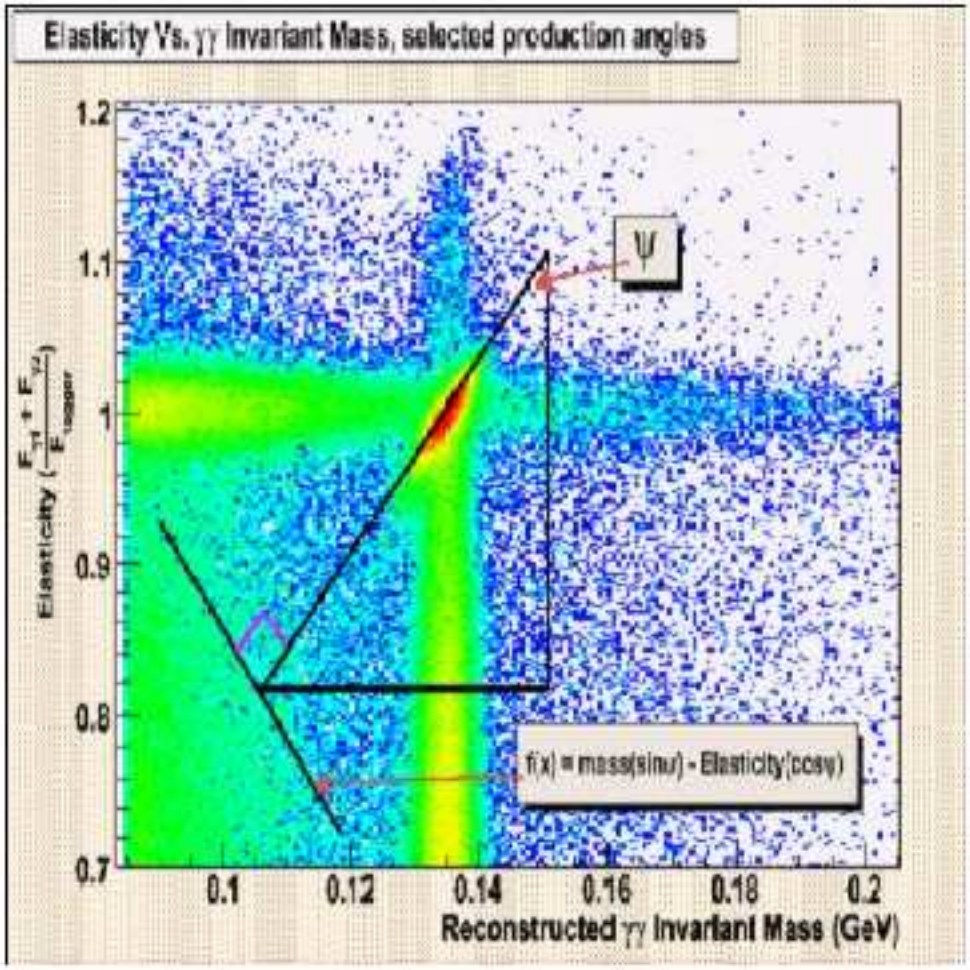
Elasticity Vs. γγ Invariant Mass, selected production angles
1.2
1.1
1
0.9
0.8
0.7
Elasticity $(\frac{E_{\gamma1}+E_{\gamma2}}{E_{beam}})$
ψ
f(x) = mass(sinω) - Elasticity(cosω)
0.1
0.12
0.14
0.16
0.18
0.2
Reconstructed γγ Invariant Mass (GeV)

Figure 2:

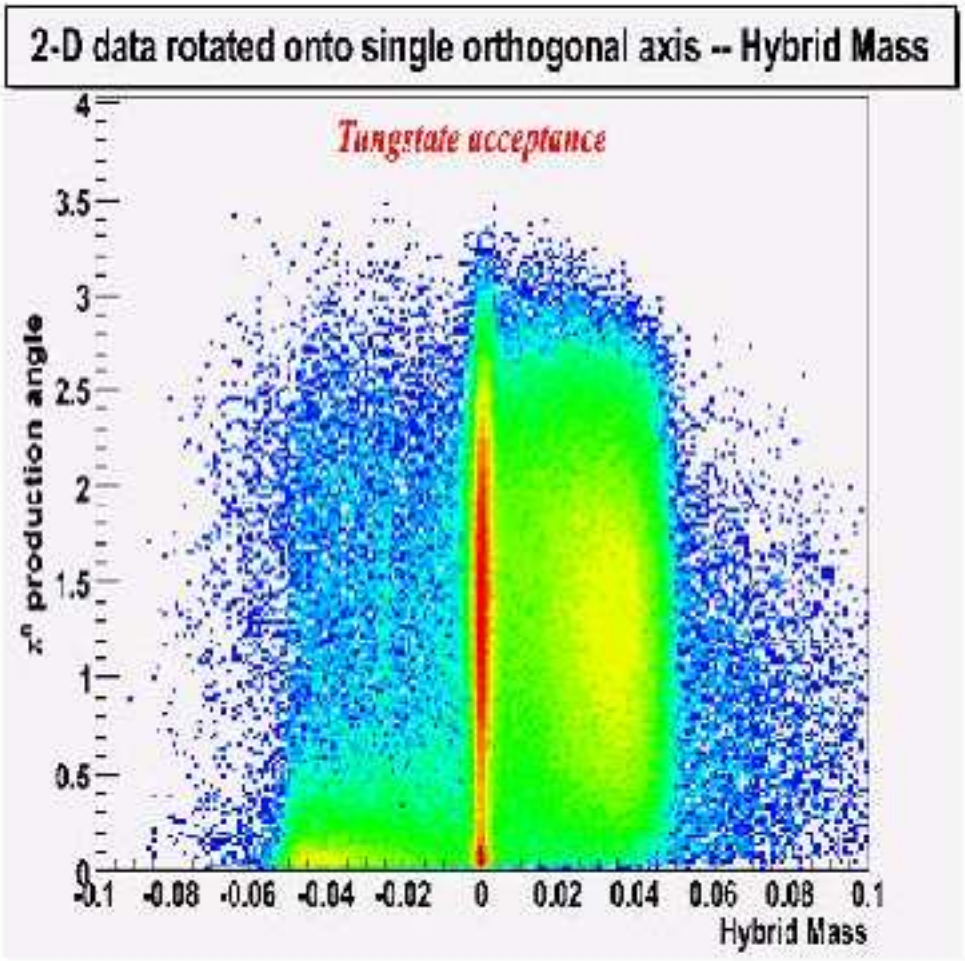
2-D data rotated onto single orthogonal axis -- Hybrid Mass
Tungstate acceptance
π^0 production angle
Hybrid Mass
4
3.5
3
2.5
2
1.5
1
0.5
0
-0.1
-0.08
-0.06
-0.04
-0.02
0
0.02
0.04
0.06
0.08
0.1

Figure 3:

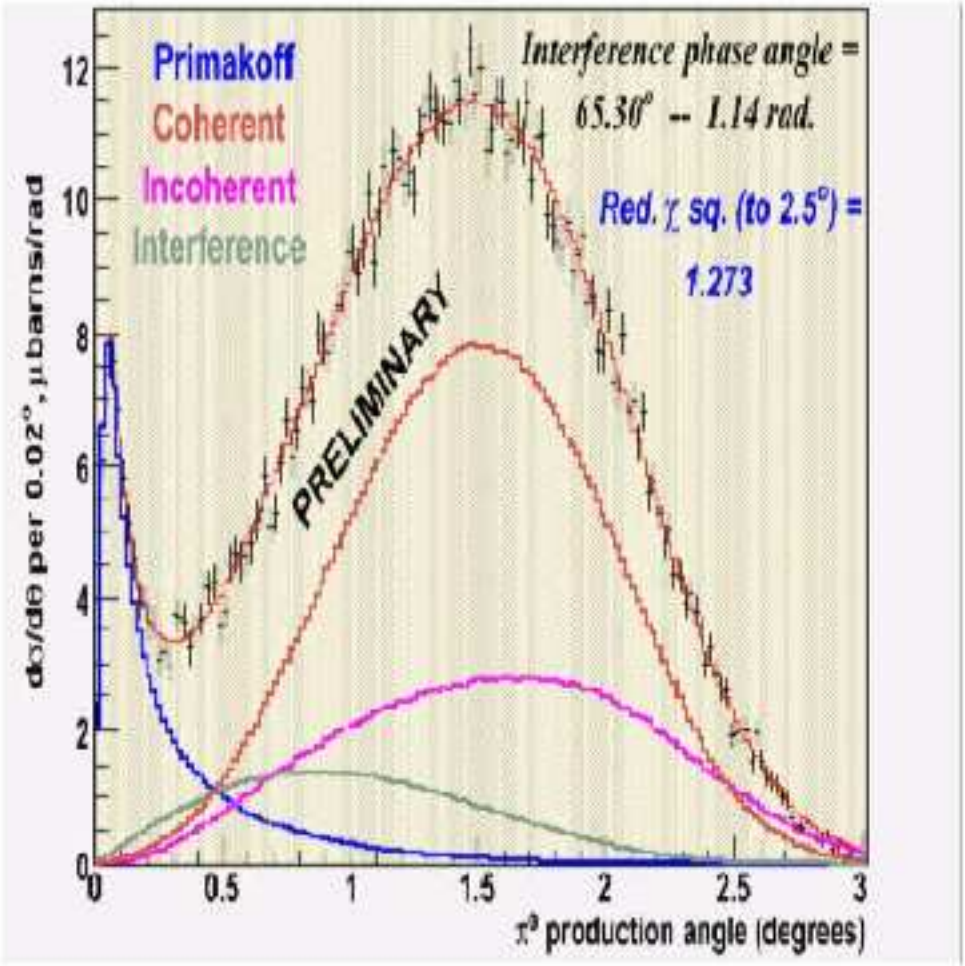
Primakoff
Coherent
Incoherent
Interference
Interference phase angle =
65.30° -- 1.14 rad.
Red. χ sq. (to 2.5°) =
1.273
PRELIMINARY
dσ/dθ per 0.02°, μbarns/rad
π⁰ production angle (degrees)
0
2
4
6
8
10
12
0
0.5
1
1.5
2
2.5
3

Figure 4:

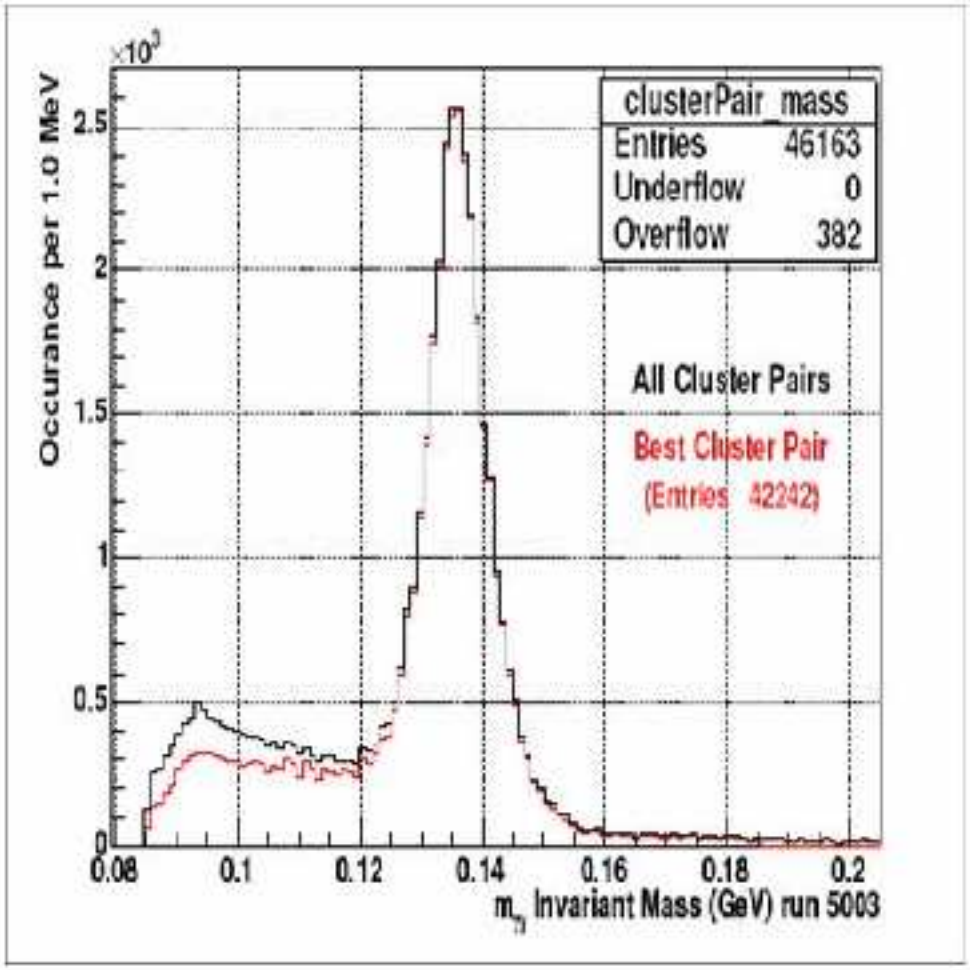
clusterPair_mass
Entries 46163
Underflow 0
Overflow 382
All Cluster Pairs
Best Cluster Pair
(Entries 42242)
Occurance per 1.0 MeV
×10³
2.5
2
1.5
1
0.5
0
0.08
0.1
0.12
0.14
0.16
0.18
0.2
m_γγ Invariant Mass (GeV) run 5003

Figure 5:

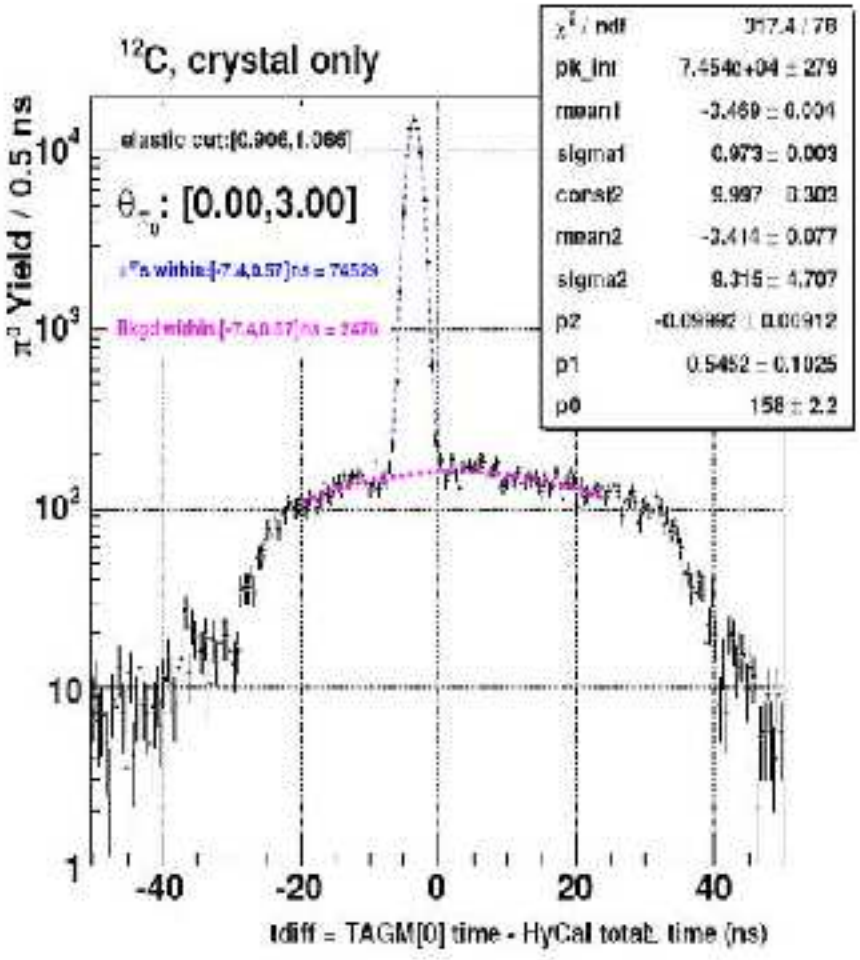
^{12}C, crystal only
elastic cut:[0.906,1.066]
θ_{π^0}: [0.00,3.00]
π^0s within [-7.4,0.57] ns = 74529
Bkgd within [-7.4,0.57] ns = 3470
χ^2 / ndf 317.4 / 78
pk_int 7.454e+04 ± 279
mean1 -3.469 ± 0.001
sigma1 0.973 ± 0.003
const2 9.997 ± 3.303
mean2 -3.414 ± 0.077
sigma2 8.315 ± 4.707
p2 -0.09992 ± 0.00912
p1 0.5452 ± 0.1025
p0 158 ± 2.2
π^0 Yield / 0.5 ns
10^4
10^3
10^2
10
1
-40
-20
0
20
40
tdiff = TAGM[0] time - HyCal total time (ns)

Figure 6:

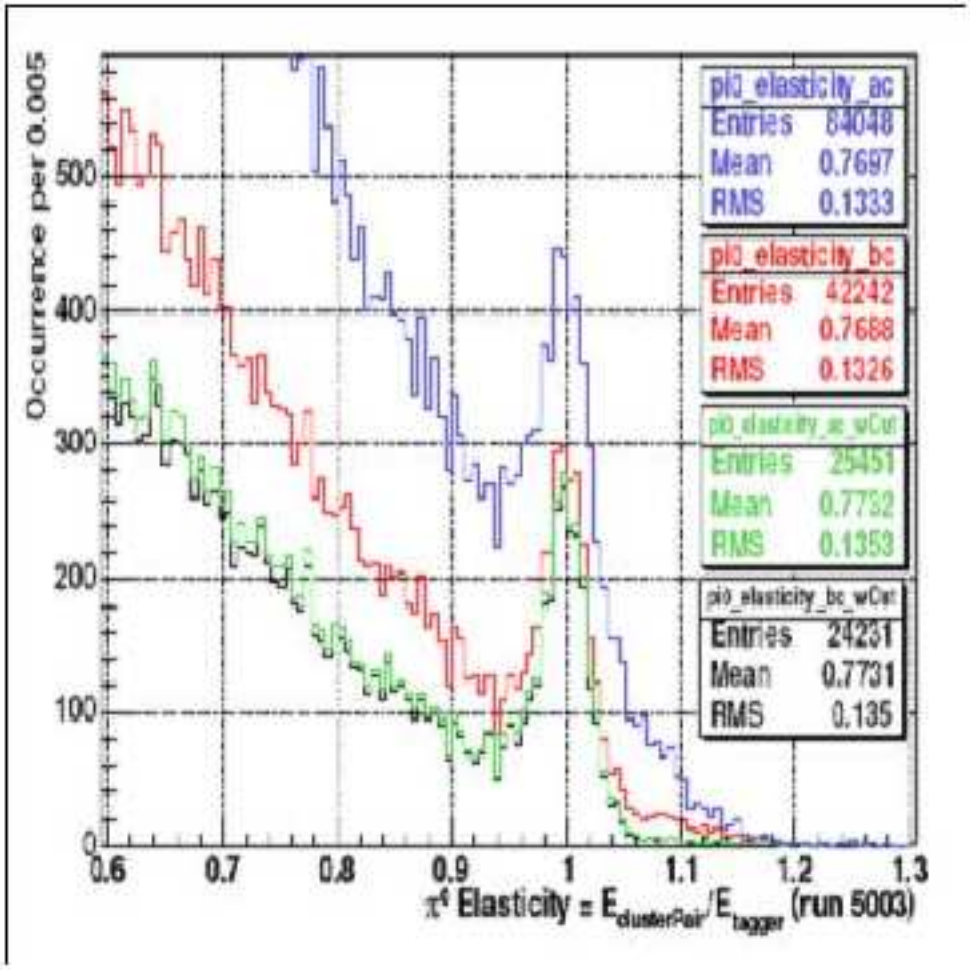
pi0_elasticity_ac
Entries 84048
Mean 0.7697
RMS 0.1333
pi0_elasticity_bc
Entries 42242
Mean 0.7688
RMS 0.1326
pi0_elasticity_ac_wCut
Entries 25451
Mean 0.7752
RMS 0.1359
pi0_elasticity_bc_wCut
Entries 24231
Mean 0.7731
RMS 0.135
Occurrence per 0.005
0
100
200
300
400
500
0.6
0.7
0.8
0.9
1
1.1
1.2
1.3
π⁰ Elasticity = E_clusterPair/E_tagger (run 5003)

Figure 7:

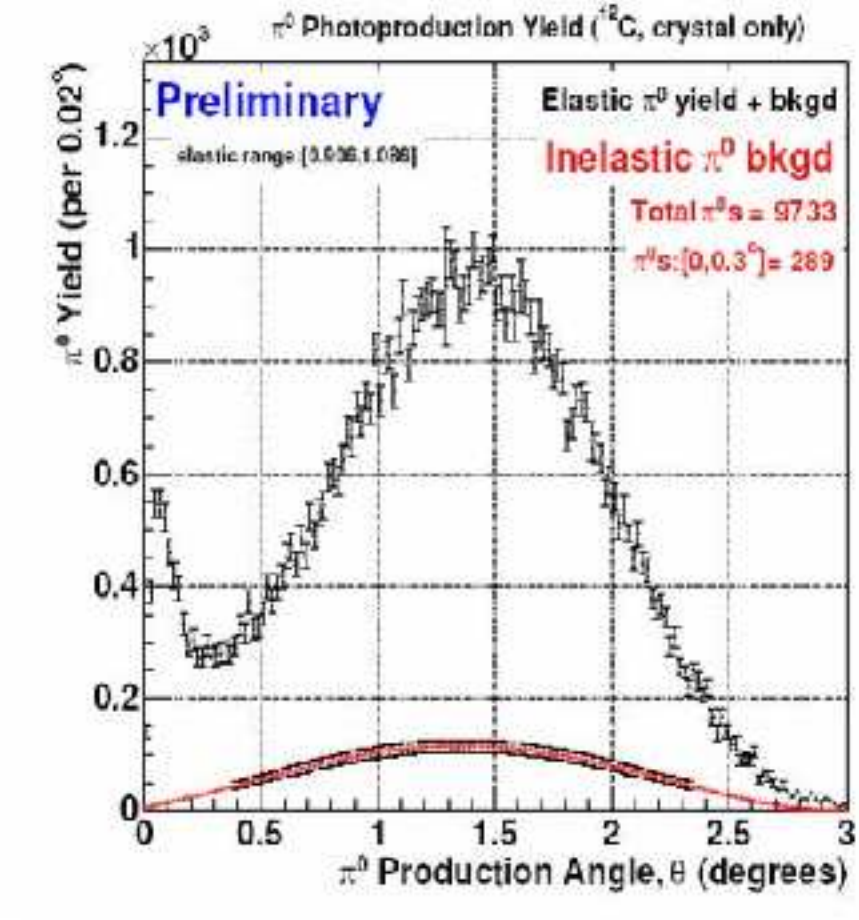
π^0 Photoproduction Yield (^{12}C, crystal only)
$\times 10^3$
Preliminary
Elastic π^0 yield + bkgd
Inelastic π^0 bkgd
Total π^0s = 9733
π^0s:[0,0.3°]= 289
π^0 Yield (per 0.02°)
π^0 Production Angle, θ (degrees)
0
0.2
0.4
0.6
0.8
1
1.2
0.5
1.5
2
2.5
3

Figure 8:

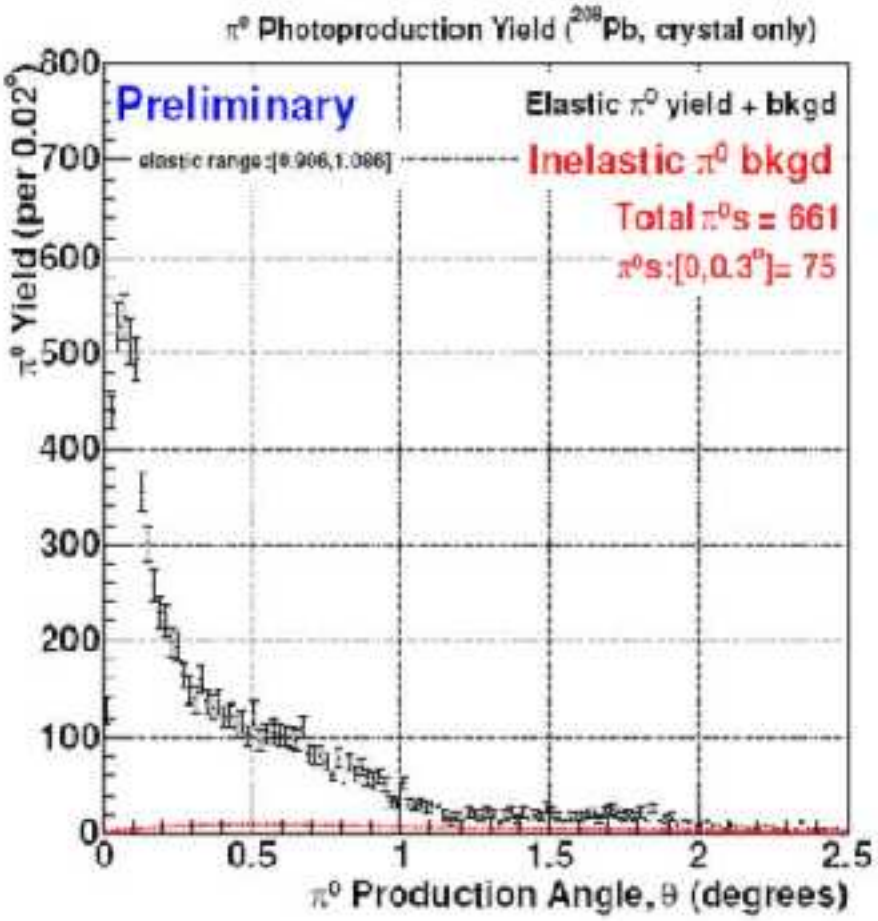
π⁰ Photoproduction Yield (208Pb, crystal only)
Preliminary
Elastic π⁰ yield + bkgd
elastic range:[0.906,1.086]
Inelastic π⁰ bkgd
Total π⁰s = 661
π⁰s:[0,0.3°]= 75
π⁰ Yield (per 0.02°)
π⁰ Production Angle, θ (degrees)
0
100
200
300
400
500
600
700
800
0
0.5
1
1.5
2
2.5

Figure 9:

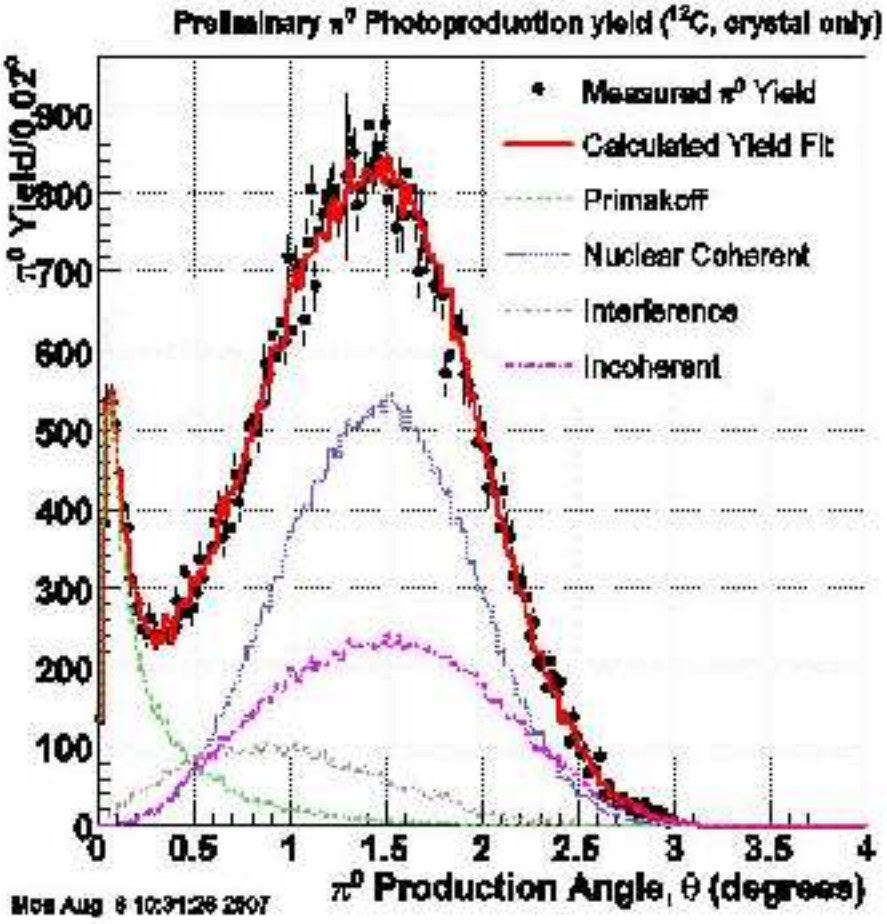
Preliminary π⁰ Photoproduction yield (¹²C, crystal only)
Measured π⁰ Yield
Calculated Yield Fit
Primakoff
Nuclear Coherent
Interference
Incoherent
π⁰ Yield/0.02°
π⁰ Production Angle, θ (degrees)
Mon Aug 6 10:31:26 2007

Figure 10:

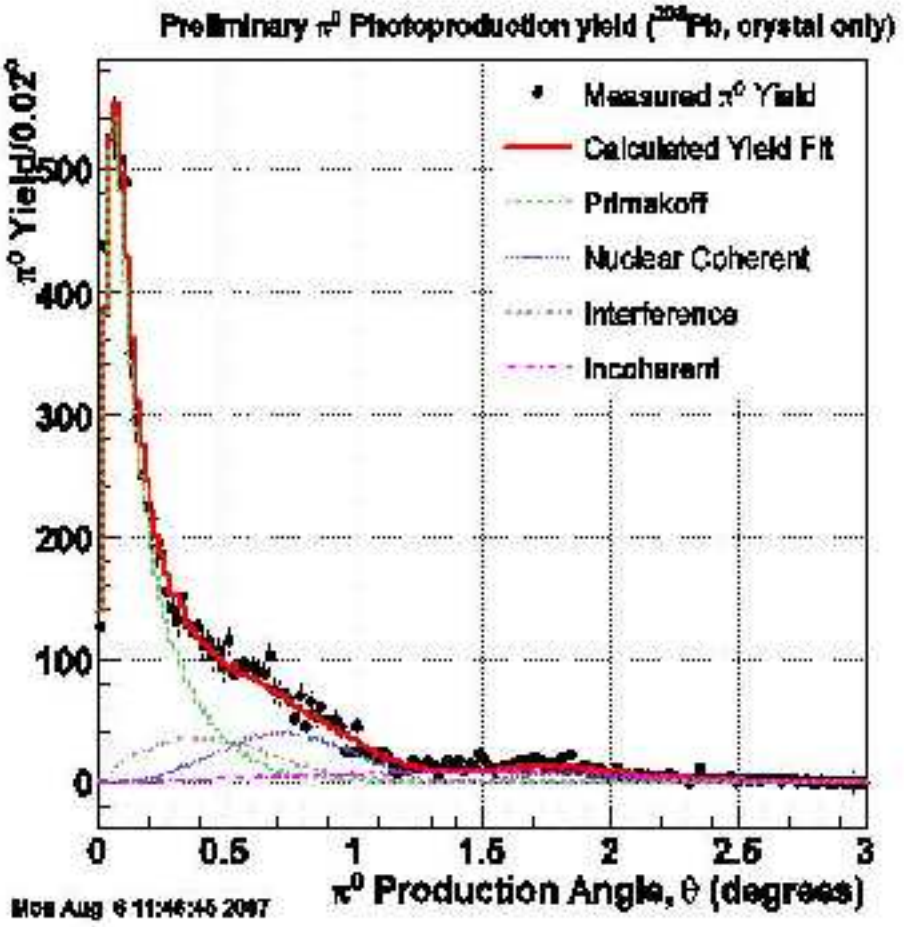
Preliminary π⁰ Photoproduction yield (²⁰⁸Pb, crystal only)
Measured π⁰ Yield
Calculated Yield Fit
Primakoff
Nuclear Coherent
Interference
Incoherent
π⁰ Yield/0.02°
500
400
300
200
100
0
0
0.5
1
1.5
2
2.5
3
π⁰ Production Angle, θ (degrees)
Mon Aug 6 11:46:45 2007

Figure 11:

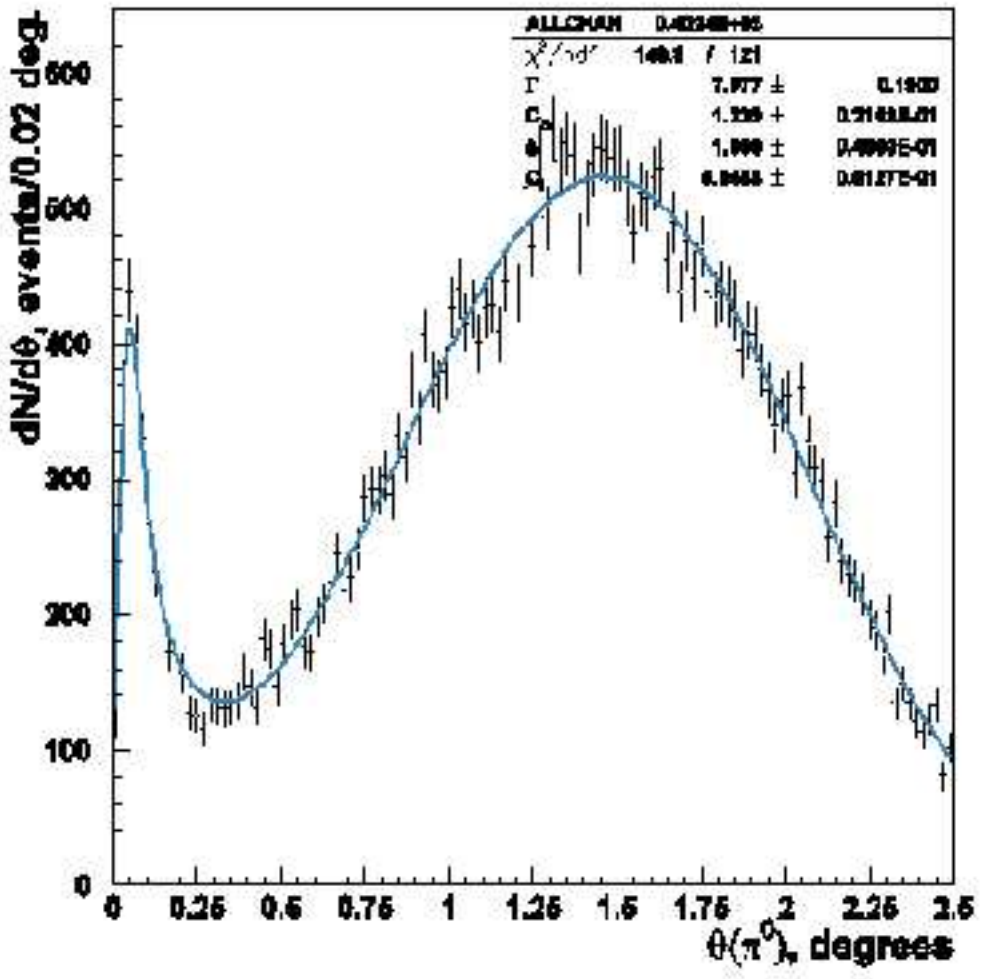
dN/dθ, events/0.02 deg.
θ(π⁰), degrees
0
100
200
300
400
500
600
0
0.25
0.5
0.75
1
1.25
1.5
1.75
2
2.25
2.5

Figure 12:

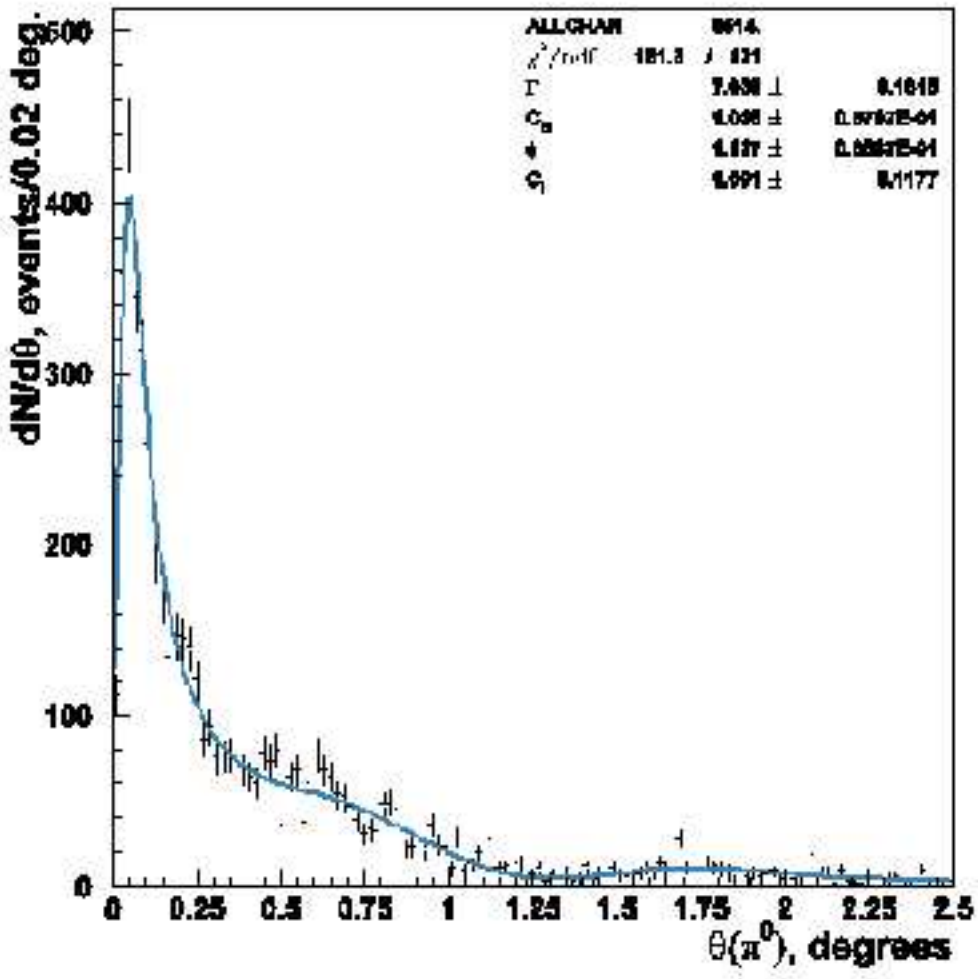
ALLCHAR
Γ
dN/dθ, events/0.02 deg.
θ(π⁰), degrees
0
100
200
300
400
500
0.25
0.5
0.75
1
1.25
1.5
1.75
2
2.25
2.5

Figure 13:

5.3 Luminosity monitoring

The primary advantages of the *PrimEx* experiment over the previous Primakoff experiments arise from the use of the Jefferson Lab Hall-B photon tagging facility to carefully control systematic errors and reduce backgrounds. First, the tagging technique allows for a significantly more accurate knowledge of the photon flux. Second, due to the energy dependence of the Primakoff cross section, it is critical to have a good knowledge of the absolute photon beam energy.

In order to determine the energy of the decaying π^0, each event is recorded in coincidence with a signal from the tagger. The experimental cross section for neutral pion photo-production is given by the following expression:

$$\frac{d\sigma}{d\Omega} = \frac{dY_{\pi^0}^{tagged}}{N_\gamma^{tagged} \cdot \epsilon \cdot t \cdot d\Omega} \tag{1}$$

where $d\Omega$ is the element of solid angle of the pion detector, $dY_{\pi^0}^{tagged}$ is the yield of tagged π^0-s within solid angle $d\Omega$, t is the target thickness, ϵ is a factor accounting for geometrical acceptance and energy dependent detection efficiency and N_γ^{tagged} is the number of *tagged* photons on the target (the tagged photon flux.

As can be seen from Equation 1 the normalization of the cross section directly depends on knowing the photon flux on the target. A naive assumption, that the number of tagged photons on target is equal to the number of hits recorded by the tagging counters, is not true because of a number of effects:

(1) events in which a bremsstrahlung photon is produced and then absorbed before reaching the target.

(2) Moller scattering events in the bremsstrahlung radiator which produce an electron in the tagging counters without an accompanying photon.

(3) extra hits registered in the tagging counters due to room background.

To minimize the absorption of photons before they reach the target, the bremsstrahlung beam travels in vacuum. The Moller scattering events are known to affect the tagging rate at the level of a few percent. The impact of the room background on the tagging rates of runs with various electron beam intensities is non-trivial and therefore continuous and attentive monitoring is necessary.

The combination of these effects can be measured in a calibration run by removing the physics target and placing a lead-glass total absorption counter (TAC) directly in the photon beam. Assuming that the total absorption counter is 100% efficient in detecting photons in the energy range relevant for the experiment,TAC the ratio of Tagger·TAC coincidences to the number of tagger hits, the so called absolute tagging ratio, is then recorded:

$$R_{absolute} = \frac{N_{\gamma e}^{TAC}}{N_e}|_{calibration} \tag{2}$$

where $N_{\gamma e}^{TAC}$ is the number of photons registered by the TAC in coincidence with a tagging signal and N_e is the number of electrons registered in tagging counters.

Knowing this ratio, one can determine the tagged photon flux in the data taking run by counting the number of post bremsstrahlung electrons in the tagging counters:

$$N_{\gamma}^{tagged}|_{experiment} = N_{e}|_{experiment} \times R_{absolute} \tag{3}$$

The use of the total absorption counter to calibrate the number of tagged photons per electron in the tagger provides an absolute normalization of the photon flux incident on the π^0 production target. However, these measurements can be performed only at intervals between the data taking. Also in the calibration run, the rate of the total absorption counter is limited, and therefore, the tagging ratio can only be measured at a rate which is reduced by a factor of about one thousand as compared to the data taking run. As such, any rate and time dependence in the tagging efficiency must be carefully considered. Consequently, a pair production luminosity monitor was constructed (see Section ??) which is able to measure the relative tagged photon flux over a range of all relevant intensities, and operate continuously throughout the data taking runs. The PS uses the physics target as a converter to measure the ratio of the number of $\gamma + A \rightarrow A + e^+ + e^-$ reactions in coincidence with a tagging signal to the number of hits in the tagging counters (see Equation 4),

$$R_{relative} = \frac{N_{e^+e^-e}^{PS}}{N_{e}} \tag{4}$$

while this is a relative number, its absolute normalization can be fixed with the TAC.

The advantages of the pair spectrometer are that it can operate over the entire range of intensities (of both the flux calibration and data taking runs) and has a smooth, relatively flat acceptance in E_{γ} covering the entire tagging range. The segmentation of the pair spectrometer detectors is driven by the fact that the pair production and Primakoff target are the same, and therefore the pair spectrometer detectors must accommodate the rates from a 5% radiation length target. Under the PrimEx run conditions, we had singles rates on a single telescope of about 140kHz, and a total of 90kHz of $PS \cdot Tagger$ coincidences over the range of tagging energies. The efficiency of the pair spectrometer for tagging photons was about 0.45%.

The PrimEx experiment is intended to provide a measurement of the π^0 lifetime with better than 1.5% precision. As quoted in the error budget of the experiment (see [?]), the main contribution to the error bar in the PrimEx measurement comes from the knowledge of the photon flux. To achieve the desired precision in the measurement of the π^0 decay width it is necessary to know the photon flux to 1% or better. To emphasize the importance of the photon flux measurement for the *PrimEx* experiment it should be noted that such a high precision measurement of the photon flux has not been previously attempted at Jefferson Lab Hall-B. Given by Equation 3 the problem of cross section normalization is reduced to the determination of the number of electrons in tagging counters and measuring the absolute tagging ratio. The constant online monitoring of the relative photon flux is also very crucial for the precision tagged photon flux measurement.

Note that in Equation 1 the $Y_{\pi^0}^{tagged}$ and N_{γ}^{tagged} need to be carefully defined. As it is defined above, $Y_{\pi^0}^{tagged}$ is the total number of π^0 events induced by *tagged* photons, and *not* the total number of π^0 events observed by HyCal. To reduce the data acquisition rates the primary trigger is not induced by the tagged photons, but by the HyCal, which means there

are possible π^0 events in the data which are induced by untagged photons. These π^0 events, which do not have "partner" electrons in the tagger have essentially no capability to pass the energy conservation requirement which is used to reduce the backgrounds. Thus these events are excluded from consideration. In the yield we count only π^0 events which are tagged as true events. The N_γ^{tagged} in the denominator of Equation 1 has to be counted consistently with the way $Y_{\pi^0}^{tagged}$ is estimated. Meaning that if for any reason events are discarded from yield calculation they should not be considered when calculating the photon flux either and vice versa.

The fact that for the cross section measurement we are interested only in tagged pion yield, *i.e.* number coincidences of π^0 and tagging electron, and tagged photon flux, which is proportional to the number of tagging electrons, results in a convenience of not having to worry about the detection efficiency of tagging counters and the deadtime effects of the data acquisition. Due to the tagged nature of the yield and the photon flux both, the efficiency of tagger and the deadtime, appear in the numerator as well as in the denominator when calculating the cross section such that the effect cancels out. But keep in mind that this does not necessarily include inefficiencies which can be introduced through the reconstruction software. A more detailed discussion will follow in Chapter 6.

5.3.1 Absolute tagging ratios

During *PrimEx* data taking, in the Fall of 2004, specialized calibration runs were periodically performed to determine the absolute normalization of the photon flux. For a calibration run, the experimental target is retracted and a Total Absorption Counter (TAC) is placed in the path of the photon beam. To avoid the radiation damage to the TAC, the electron beam intensity is lowered to $\sim 70 - 80pA$. The low intensity of calibration runs enables the use of the Tagger Master OR (MOR) signal as the data acquisition trigger. The MOR signal is formed by OR-ing the timing information from all or any of the 61 T-counters. Using the MOR trigger enables one to directly count the number of electrons that hit the tagging counters. Due to the reduced intensity of the primary beam, even a slight variation in room background can have a significant negative effect on the tagging ratios. Thus periodic measurements are necessary to ensure a stable, reproducable result. As discussed in Section ?? the T-counters have overlapping geometrical acceptances and non-overlapping T-channels are defined via timing coincidences. Due to the small size of the overlaps, the rates in the even channels are low (see Figure ?? Parts (a) and (b)), so in order to obtain sub-percent statistical errors within a reasonable amount of time the even channels are grouped together with the previous odd channel to form "combined T-channels" as shown in Figure 14.

Absolute tagging ratios are then defined for each of the T-counters as:

$$R^i_{absolute} = \frac{N^{TAC}_{\gamma e^i}}{N^i_e} \tag{5}$$

where N^i_e is the number of electrons registered in the T-counter i and $N^{TAC}_{\gamma e^i}$ is the number of photons registered by the TAC in coincidence with an electron in the T-counter i.

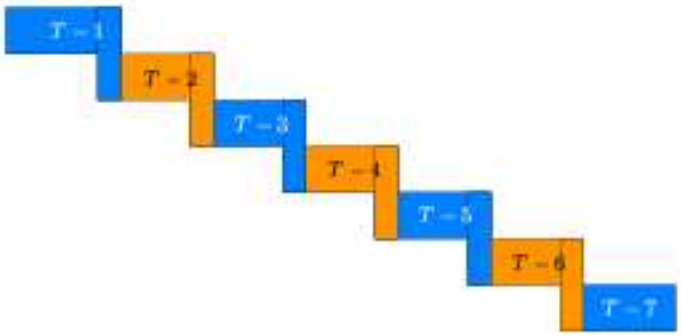

Figure 14: The numbering scheme of the combined T-channels, only the first 7 counters are shown.

5.3.2 Effects of incident electron beam intensity on absolute tagging ratios

As it was previously discussed, due to the techical limitations of the TAC the absolute tagging ratios can be measured only at beam intensities which are $\sim 10^3$ times lower than the intensity of a regular production run. The goal of PrimEx is to be able to measure the photon flux for the production data with a precision of 1% or better. It is important to demonstrate that the tagging efficiencies obtained at beam intensities of $\sim 80pAmps$ are valid when applied to the data collected at the high beam intensities of about 80 to 130 $nAmps$. To investigate this, during our running period in Fall of 2004 we had normalization runs with various beam intensities ($40 - 120pAmps$).

Figure 15 (top) shows the absolute tagging ratios as a function of T-counter number measured at different beam intensities. An artificial shift was introduced on the horizontal axis in order to be able to distinguish the different measurements. As a result, one has 11 groups of 4 points (one group per T-counter). The weighted average was calculated for each of the 11 groups. Figure 15 (bottom) shows the percent deviation of each measurement from the mean value for the relevant group. No noticeable systematic dependence of tagging ratios on the incident beam intensity was detected when varying the beam intensity from $40pAmps$ to $120pAmps$.

5.3.3 Effects of collimator size

A decision was made for *PrimEx* to run with very loose collimation of the bremsstrah-lung photon beam to cut out the beam halo. Together with careful monitoring of the beam position, collimation should increase the stability of the luminosity by keeping the photon beam focused at one spot on the target and thus reducing the effects of possible nonuniformity of the target thickness.

Two different sizes of copper collimators were available for this purpose. In Figure 16 (top) the relative tagging ratios are plotted versus T-counter ID for data taken with 2 different collimators. For reference purposes a result with no collimation is also plotted. For these measurements, the statistical error on each point is on the order of 0.15%. It is easy to see from Figure 16 (bottom) that the $12.7mm$ collimator cuts out $\sim 1\%$ of the photon beam and $8.6mm$ collimator cuts out $\sim 4\%$ of the photon beam.

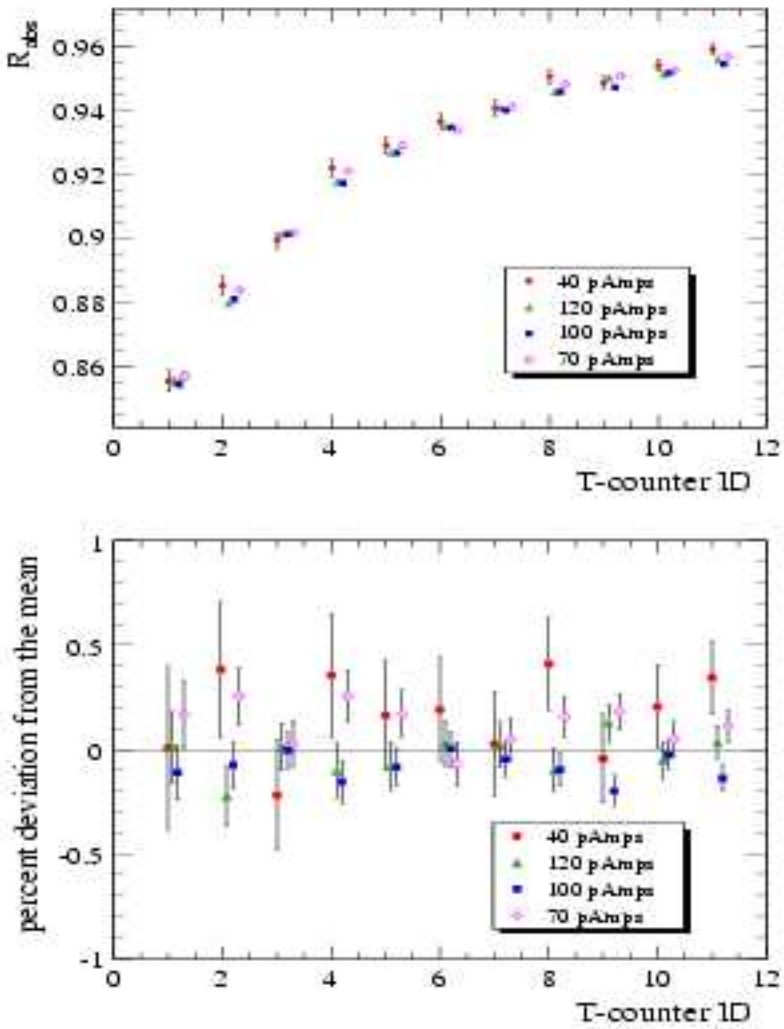

Figure 15: (top) Absolute tagging ratios plotted as a function of T-counter number for runs with different beam intensities, (bottom) The percent deviations from the mean for tagging ratio measurements made at different beam intensities for the first 11 T-counters.

5.3.4 Effects of collimator position misalignment

Figure 17 shows the position of the collimator on its ladder versus run number. One can easily see that the entire running period can be divided up on two groups of runs. The group 1) with run numbers from 4100 to 4295 with collimator at $7.075in$ and the group 2) with run numbers from 4502 to 5447 with collimator at $7.02in$. Keeping in mind the required precision of 1% on the photon flux, it is important to investigate the extent to which the tagging ratios are affected by this shift.

The tagging ratios measured for 5 different positions are shown on Figure 18 (top). Figure 18 (bottom) shows the percent deviation of tagging ratios, measured at different positions of the collimator, from the value which was measured with the collimator in its

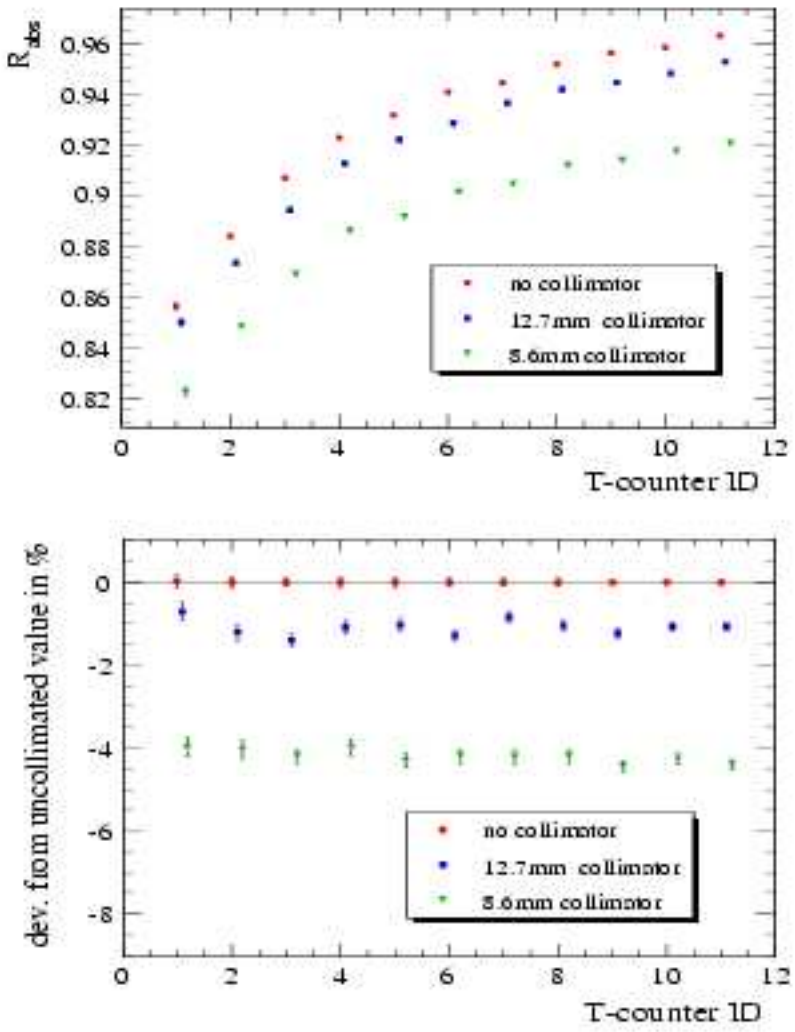

Figure 16: (top) R_{abs}, measured for 3 different collimator sizes, (bottom) Percent deviation from the uncollimated value.

nominal position (*i.e.* at $7.02in$). From Figure 18 (bottom) one can easily see that the shift in collimator position from $7.02in$ to $7.15in$ ($\sim 3.3mm$) lowers absolute tagging ratios by about 0.34%, hence if needed runs 4549, 4326, 4327 can all be used when calculating the final tagging ratios to reduce the the statistical error. One can also notice that larger shifts in collimator position result in $\sim 1.2\%$ and more reduction of R_{abs}.

5.3.5 Effects of HyCal scraping due to beam mis-steering (uncollimated beam)

As described in Section ?? the space between the Pair Spectrometer dipole vacuum window and the face of HyCal is taken up by a helium bag. The HyCal has a central opening to allow the uninteracted beam particles to pass through. A **G**amma **P**rofiler (GP) was installed directly behind the calorimeter to monitor the shape and the position of the photon beam

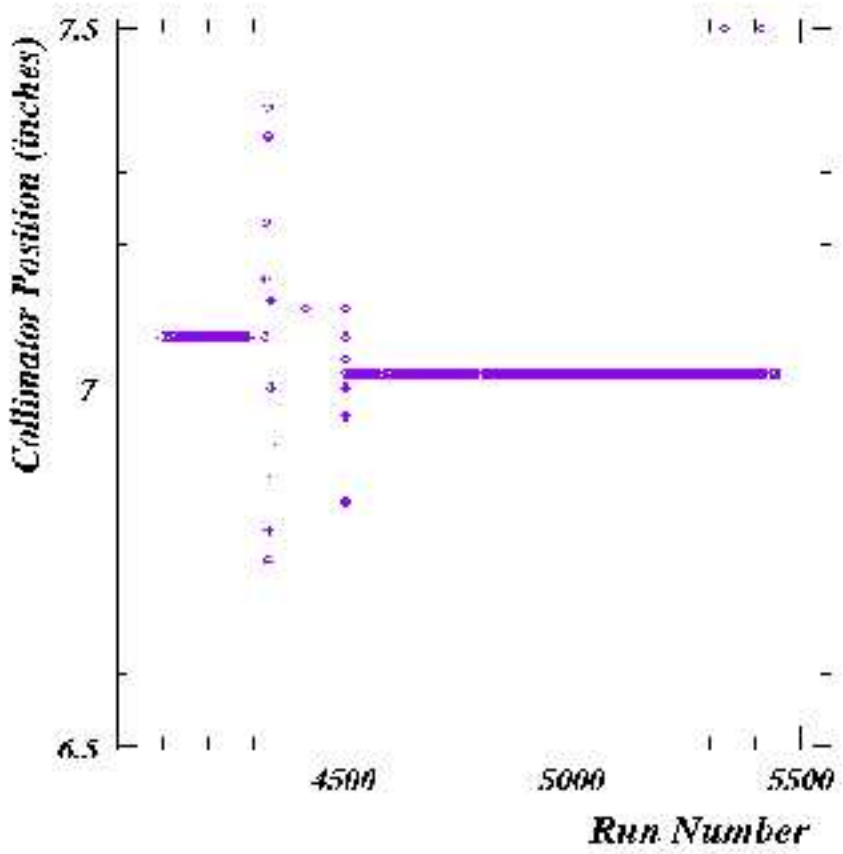

Figure 17: collimator position vs. run number.

during the experiment. Ideally one would place the TAC right at the position of the target but given the technical constraints in case of PrimEx, the TAC was mounted on the same moving platform as the GP behind HyCal and was placed in the path of the photon beam interchangibly with the GP to perform a normalization run. In this configuration the photons must travel through a $4.15 \times 4.15 cm^2$ central opening in HyCal (see Section ??) before they can be registered in the TAC. Consequently it is necessary to evaluate to what extent the size of the HyCal central opening and the alignment of the photon beam with respect to the HyCal axis affect the results of normalization runs. For this purpose the direction of the photon beam was purposefully altered and the tagging ratios were measured. To allow for larger artificial shifts in beam position the collimator was retracted during this study. Due to the fact that this investigation was done with uncollimated beam it places an upper limit on the amount of the photon beam that can be cut by HyCal due to scraping. Because the GP was mounted on the same moving platform as the TAC, photon beam position measurements were possible only before and after a normalization run. In light of this, the study described in this section should be considered only as qualitative exercise.

It was determined that in the absolute coordinate system of the GP, the nominal photon beam position is: $X_{av} = -0.83mm$ and $Y_{av} = -1.45mm$. Figure 19 (top) shows several measurements of tagging ratios with different beam positions. Run # 4338 was taken with

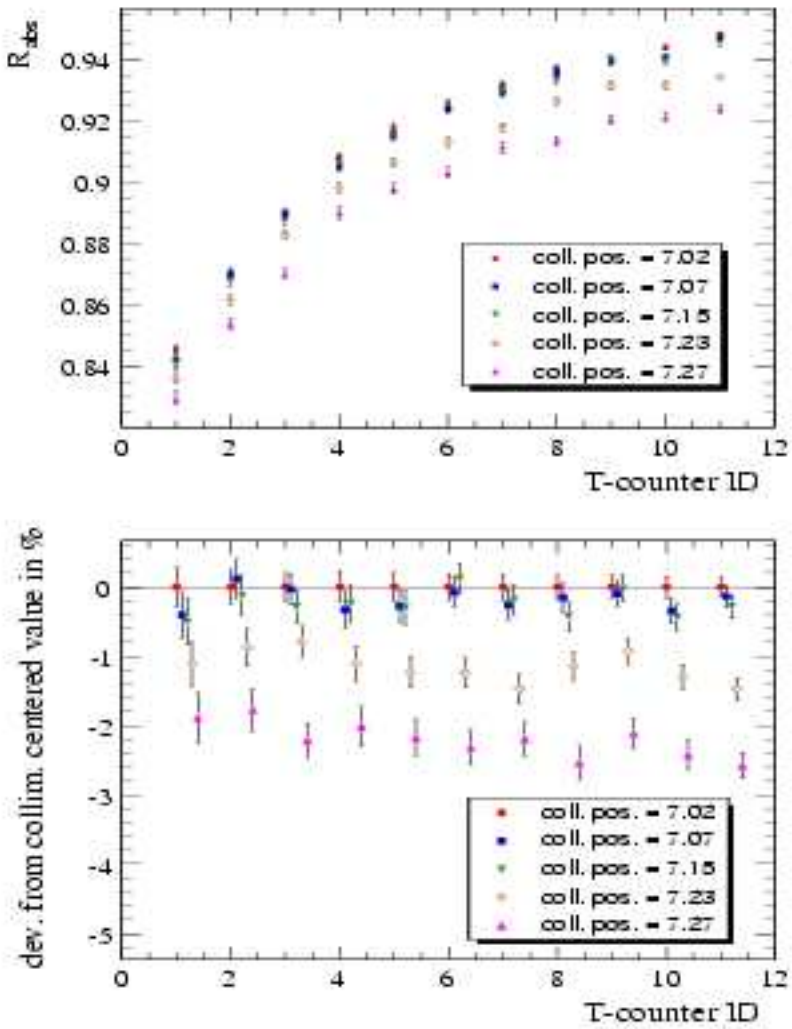

Figure 18: (top) R_{abs} measured for 5 different collimator positions measured in inches. (bottom) Percent deviation from the measurement taken with collimator in its nominal position ($7.02in$).

the beam at its nominal position. For run # 4340 the beam was steered a little over $5mm$ in positive Y direction to $(-0.93, 4.09)$. For run # 4341 the beam was at $(-6.54, -1.23)$. During run # 4342 beam was at $(-9.45, -1.52)$ – *i.e.* about $8.5mm$ off of its nominal position. For run # 4343 beam was at $(5.12, -1.44)$ – *i.e.* about $6mm$ off of its nominal position.

This qualitative study indicates that the HyCal and the beam were not positioned ideally with respect to each other. Runs # 4342 and 4343 indicate that a $\sim 8.5mm$ shift in the beam position in negative direction has the same effect on the tagging ratios as a $\sim 6mm$ shift in the positive direction along the X axis. Also runs # 4340 and 4341 indicate a slight increase ($\sim 0.23\%$) in tagging ratios when the beam is steered $5mm$ in positive Y direction or $5mm$ in negative X direction.

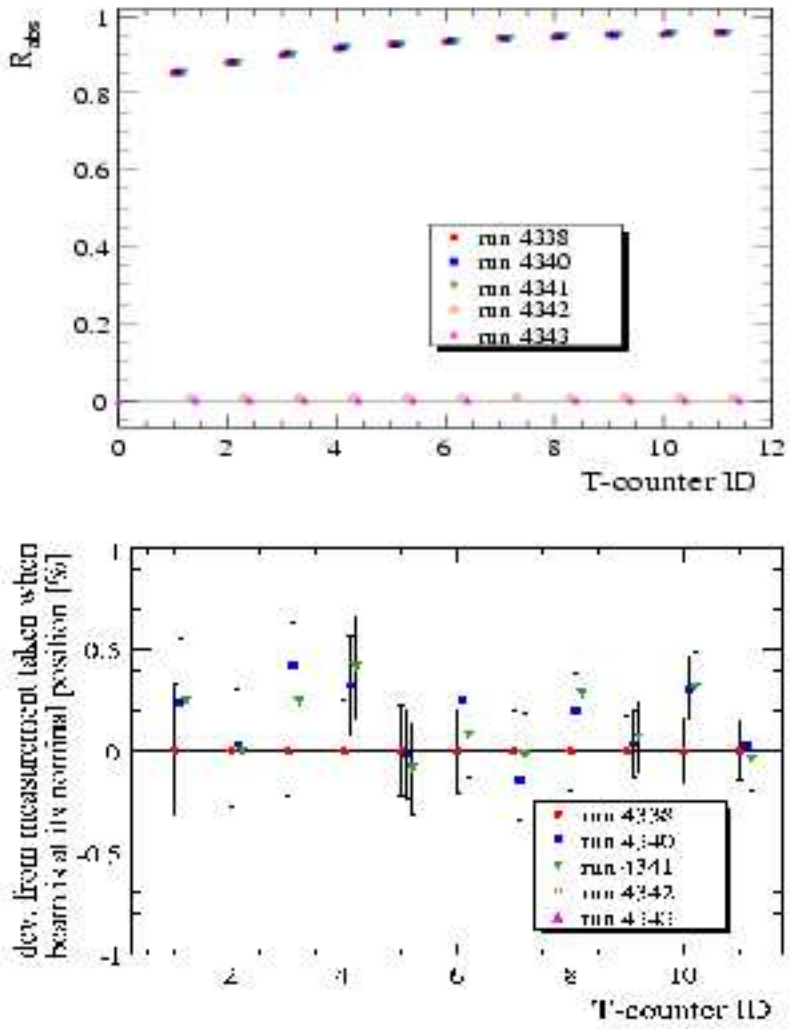

Figure 19: (top) R_{abs} measured for 5 different beam angles. (bottom) Percent deviation from the uncollimated value.

5.3.6 Long and short term reproducibility with uncollimated beam

To test our ability to perform a consistent measurement of the absolute tagging ratios, $R_{absolute}$, we had back-to-back normalization runs which were taken only $20-25$ minutes apart. The pair spectrometer magnet was operating at $\sim 900 Amps$.

As it can be seen from Figure 20, the study shows that all 4 runs agree within the limits of required precision and statistical errors.

Figure 21 (top) shows the absolute tagging ratios measured for the first 11 T-counters. These runs were taken ~ 4 and half hours and 5 days apart from each other. Figure 21

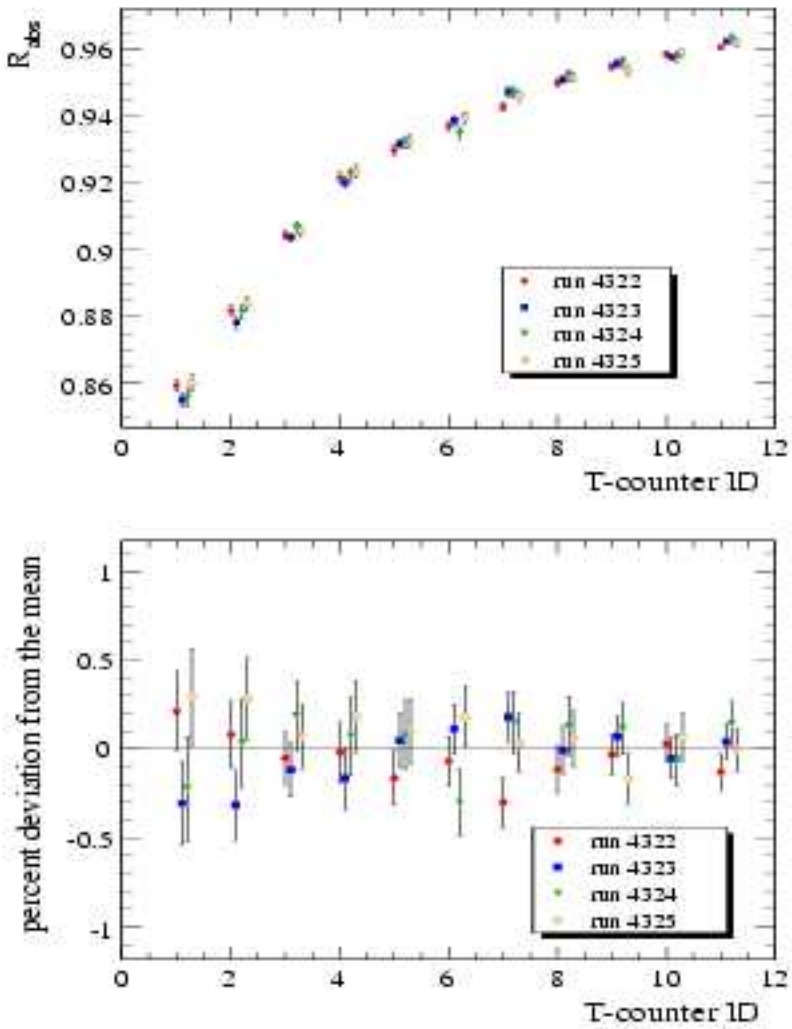

Figure 20: (top) R_{abs} measured for 4 consequtive runs. (bottom) Percent deviation from the mean.

(bottom) shows the percent deviation of the tagging ratio for each T-counter from the relevant average value. The statistical error for each point is on the order of 0.2%. As seen from the plots, all three measurements are in very good agreement with each other (better than 0.3%). Note that since since all three measurements were taken with different settings of Pair Spectrometer dipole, this study also shows that there is no detectable dependence of absolute tagging ratios on the magnetic field of the PS dipole when using an uncollimated photon beam.

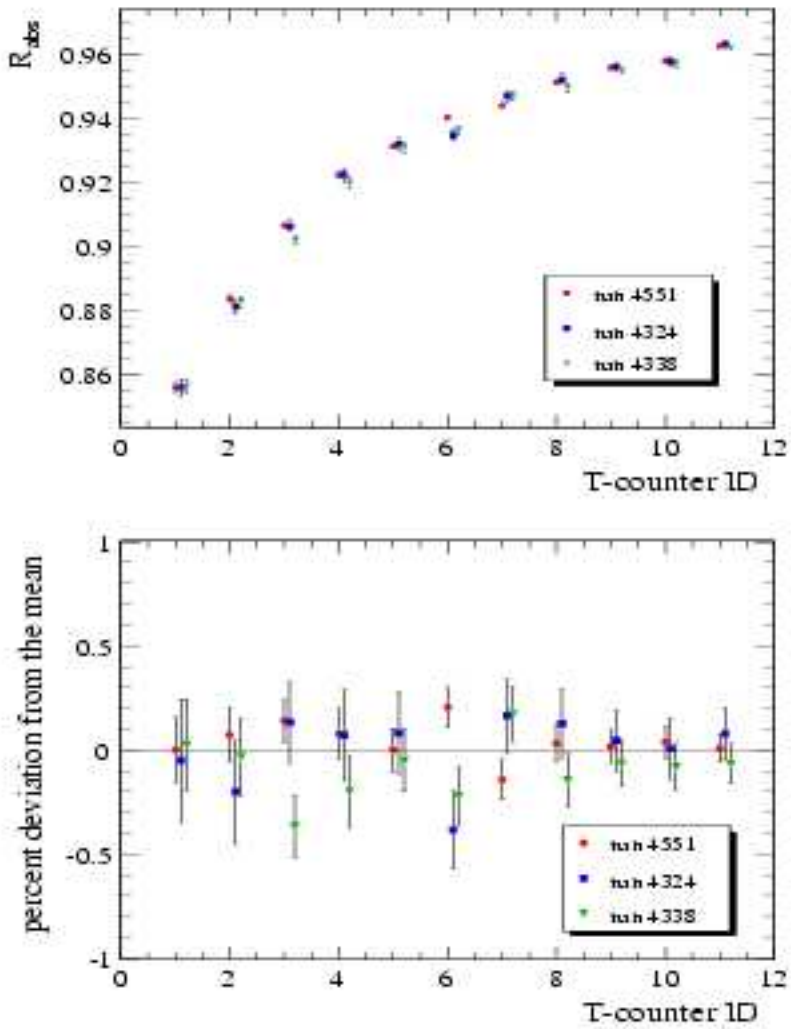

Figure 21: (top) R_{abs} measured for 3 runs which were spread in time during our data taking. (bottom) Percent deviation from the mean.

5.3.7 Effects of the PS dipole field with collimated beam

As was already demonstrated in Section 5.3.6, the PS dipole field has no measurable effect on the tagging efficiencies in the case of an uncollimated photon beam. Since, due to technical difficulties with the PS power supply, the normalization runs were performed at different values of the magnetic field of the PS dipole, and the production data for PrimEx were taken with a $12.7mm$ collimator, it is important to investigate the effect of the magnetic field on the tagging ratios measured for a collimated beam.

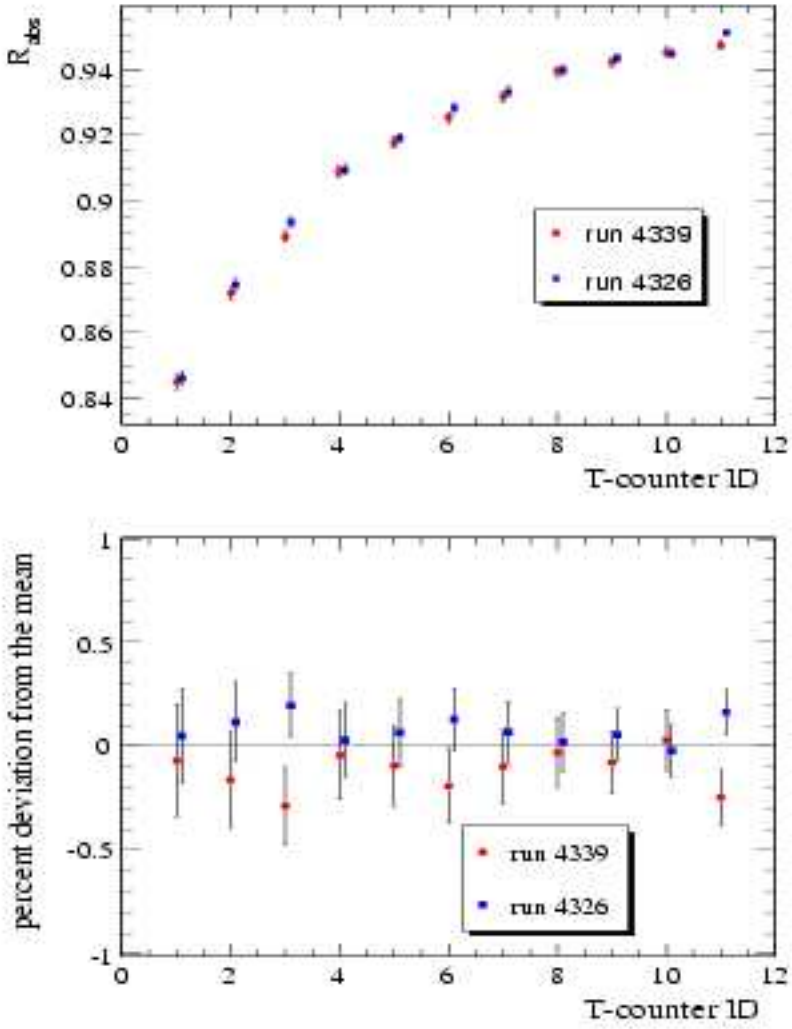

Figure 22: (top) R_{abs} measured for 2 runs which were taken with different settings of PS dipole magnet. (bottom) Percent deviation from the mean value.

5.3.8 Absorption in the target

Some of the photons are absorbed in the target without producing a π^0. Special TAC runs with a carbon target placed in the beam were performed to study this effect. Figures 23 and 24 show a comparison of tagging efficiencies measured for target in runs to those measured for target out runs for measurements performed without and with photon beam collimation. Both studies yield consistent results indicating that $\sim 3\%$ of photons are lost in the target.

Since PrimEx is aiming for a $\sim 1.5\%$ level absolute cross-section measurement one has to correct the yields for absorption of photons in the target. The main reaction of interest for PrimEx, $(\pi^0 \rightarrow \gamma\gamma)$ and the consistency check reations (Compton effect and e^+e^- production) are affected by the photon absorption in the target on different levels. In the

case of Compton and Primakoff effects not only the primary photon but also the secondary photons can be absorbed in the target. Since Compton scattering or π^0–production can happen anywhere along the longitudinal direction of the target, the result of this study can be used to set an upper limit on the effect of photon absorption.

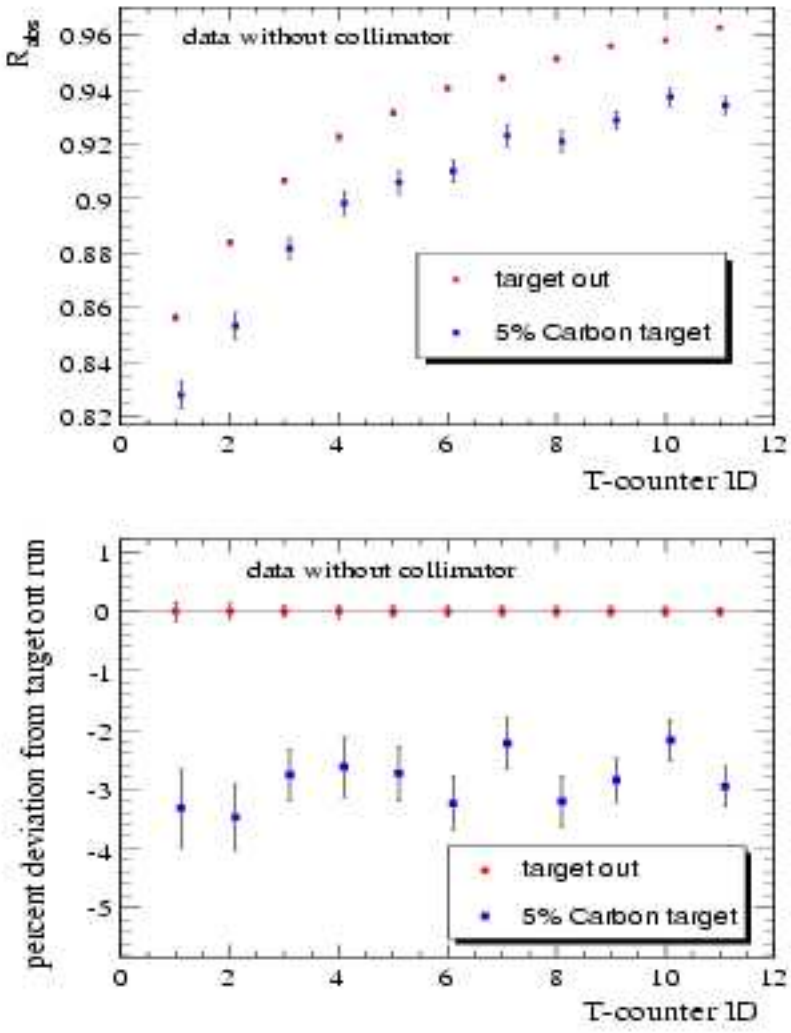

Figure 23: (top) R_{abs} measured for runs which were taken with target in and target out. (bottom) Percent deviation from the measurement obtained with physics target out; no photon collimation.

5.3.9 Relative tagging ratios measured with pair production

As described in Sections ?? and ??, the Pair Spectrometer is an essential part of PrimEx experimental apparatus designed for relative in-situ monitoring of the photon flux. The Pair Spectrometer uses the experimental target to convert a fraction of photons into e^+e^-

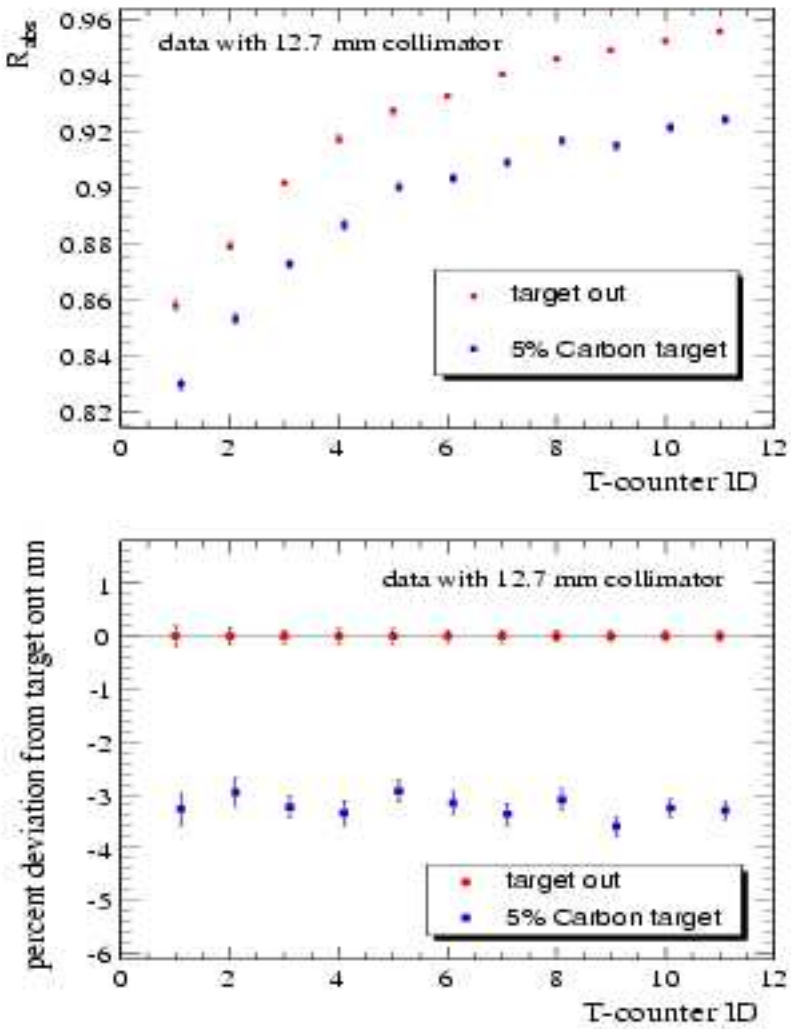

Figure 24: (top) R_{abs} measured for runs which were taken with taget in and target out. (bottom) Percent deviation from the measurement obtained with physics target out: with photon collimation.

pairs which are deflected in the field of a dipole magnet downstream of the target and are registered in plastic scintillator detectors on both sides of the beam-line. The relative tagging ratios per T-counter[1] are defined as:

$$R^{i}_{relative} = \frac{N^{PS}_{e^+e^-e^1}}{N^{i}_{e^1}} \tag{6}$$

where N_{e_1} is the number of electrons registered in T-counter i and $N^{PS}_{e^+e^-e^1}$ is the number of e^+e^- pairs registered by PS in coincidence with an electron in T-counter i.

[1]The T-counter as defined in Section ??, Figure 14.

During our production data taking, in Fall of 2004, we had random, *i.e.* not related to the particles in the beam, clock trigger set up to measure $R^i_{relative}$. The use of the random trigger allows to directly count the number of electrons in the tagging counters and it gives the advantage of being insensitive to beam intensity variations.

5.3.10 Effect of Incident Electron Beam Intensity on Relative Tagging Ratios

As it was discussed in Sections ?? and 5.3.2, the relative tagging ratios, defined by Equation 6, can be measured at low as well as at high electron beam intensities. In order to justify the use of the absolute normalization of the photon flux obtained at low electron beam intensities for calculation of the number of tagged photons on target, it is important to demonstrate the independence of the R^i_{rel} of the electron beam intensity.

In August 2002, the R^i_{rel} was measured from 0.08 to 100 $nAmps$, the results for T-counter 3 are shown in Figure 25. The data points were fitted with a first order polynomial and as can be seen R^i_{rel} is quite independent of the beam intensity (note that the $X-$ axis on top plot is presented in *log* scale).

In Figure 26 the relative tagging ratios are plotted versus T-counter ID, *i.e.* photon energy, for the data taken in Fall of 2004, over the range of electron beam intensities used in PrimEx experiment. The error on each point is not larger than 1.1%. The shape of the curve depends on factors like: setting of the Pair Spectrometer dipole magnet and the geometrical acceptance of Pair Spectrometer detectors. The pair production cross section is practically constant at the energies that are of interest to PrimEx. GEANT simulations show the same general behavior for energy dependence of R^i_{rel}.

5.3.11 Run-to-Run Stability of Relative Tagging Ratios

As it was previously discussed the relative tagging ratios have to be not only intensity independent but also stable from run to run, *i.e.* in time, to within 1%. The time stability of the relative tagging ratios measured by the PS justifies the use of a single set of absolute tagging ratios measured by the TAC for the tagged photon flux calculation. As such, to achieve a 1% level tagged photon flux measurement any deviation from nominal value of the R_{rel} has to be carefully investigated and if possible corrected for. In this and the next section the qualitative analysis of the run-to-run stability of the relative tagging ratios will be presented and possible sources for deviations will be discussed. For the purpose of this qualitative discussion the data from all 11 T-counters were combined together and the the part of the focal plane of the Tagger that is of interest to the PrimEx experiment is treated as one single counter which allows to reduce the statistical error.

Figure 27 shows the time evolution of the $R^{combined}_{rel}$ - combined relative tagging ratio in time. The two black solid lines on the graph represent $\pm 1\%$ deviation from weighted average. The weighted average for the runs with carbon target is calculated based on runs with Run Numbers less then 4800 and for lead target runs the average was determined based on the group of runs with Run Numbers from 5050 to 5090 giving for lead runs average of $0.00543505 \pm 0.0424913\%$ and for carbon runs average of $0.00505767 \pm 0.0288419\%$

It is easy to see that for the last group of runs (run number > 5150) relative tagging ratio starts to fall off. Deviation is larger than 1% and indicates that extra care is needed

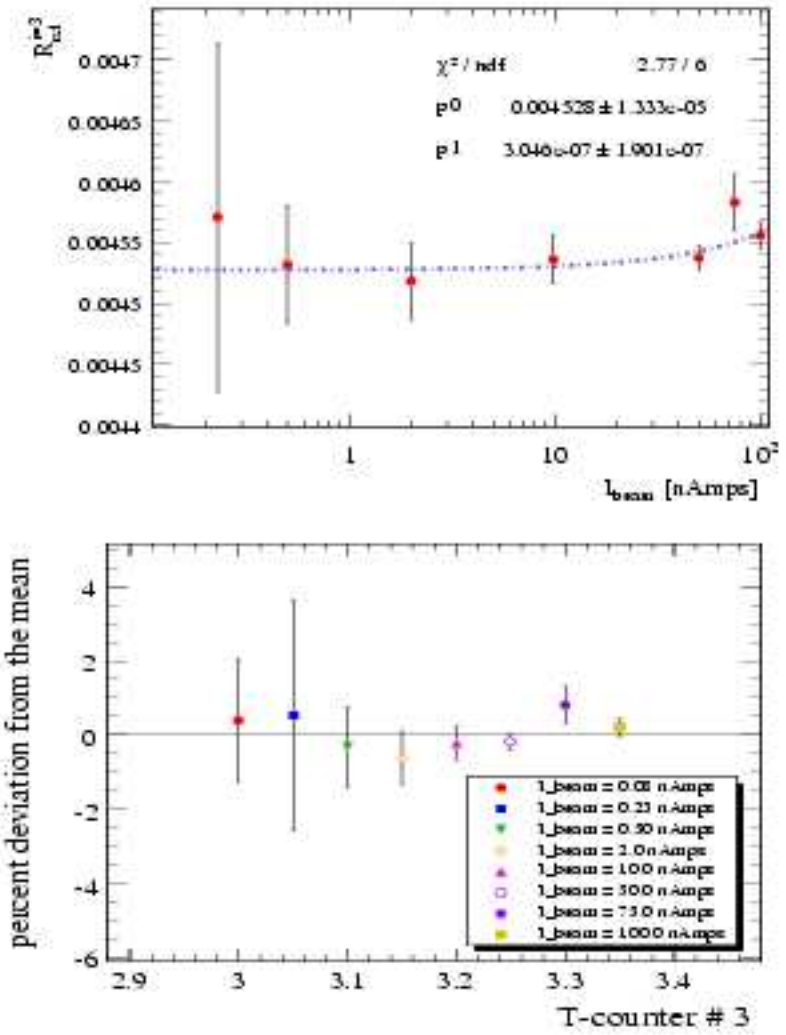

Figure 25: (top) Measured R_{tcl}^{i} for T-counter #3 as a function of nominal electron beam current. (bottom) The percent deviations from the mean for tagging ratio measurements made at different beam intensities for the first 11 T-counters.

when calculating the photon flux for this group of runs. I will try to address this issue in next two sections.

5.3.12 Inefficiency of the Tagger

Before making any corrections one needs to investigate the reason for the drop in relative tagging ratios on Figure 27. The $R_{tcl}^{combined}$ can drop due to number of reasons:

1. Tagger registers extra electrons which do not have partner photons on our physics target.

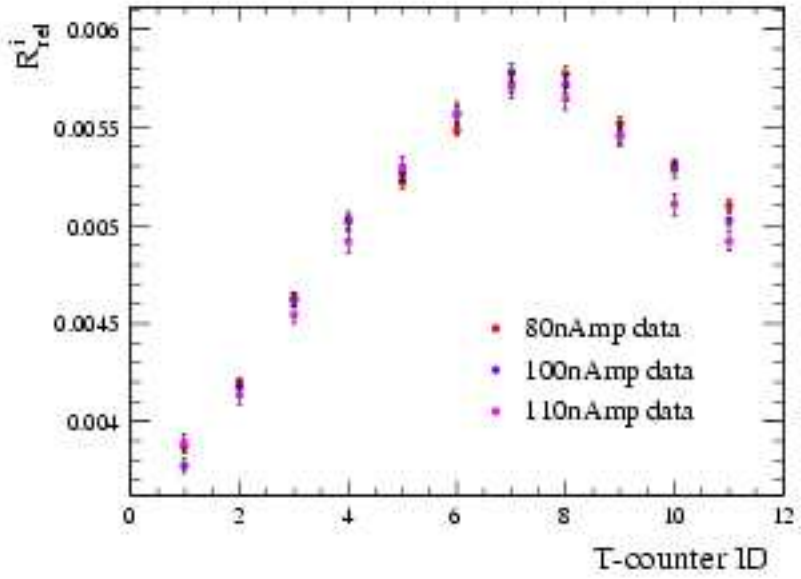

Figure 26: R^i_{rel} measured for 3 different beam currents across the focal plane of the Tagger. The radiator thickness during these measurements was $2 \times 10^{-5} X_0$.

2. A part of our photon beam is being lost before reaching the physics target (or TAC since same effect has been seen in absolute tagging ratios).

3. A combination of first two effects.

To investigate this drop in relative tagging ratios one can look at the ratio of number tagged pairs ($N^{PS}_{e^+e^-e^i}$) to the number of all pairs ($N^{PS}_{e^+e^-}$) and at the ratio of number of all pairs ($N^{PS}_{e^+e^-}$) to the number of electrons in the tagger (N^i_e).

Keeping in mind Figure 27, let us call runs $4747 - 4768$ that were taken at $\sim 80nAmps$ *group* 1, runs $4978 - 5069$ that were taken at $\sim 100nA$ *group* 2, runs $5158 - 5210$ that were taken at $\sim 130nA$ *group* 3 and runs $5211 - 5242$ that were taken at $\sim 110nA$ *group* 4.

In order to understand the beam intensity dependence of this ratios the weighted averages were calculated for each group. The results are ploted as a function of the electron beam intensity on Figures 29, 30 and 31[2]. Note that the polarity of the PS dipole field was flipped between runs in groups 1 and 2, thus the average values of only groups 2, 3 and 4 should be compared to eachother.

On Figure 29 there is a drop of 0.46% in relative tagging ratio between groups 2 and 3 (point at $130nA$). The group 4 however is $\sim 1.00\%$ lower than group 1 which indicates either drop in number of tagged e^+e^- pairs or increase in number of electrons registered in the tagger, possibly both.

Figure 30 shows a $\sim 3.52\%$ drop in $\frac{N^{PS}_{e^+e^-e^i}}{N^{PS}_{e^+e^-}}$ when going from group 2 to group 3. Note that on this plot group 4 is $\sim 2.24\%$ higher than group 3, which indicates that on Figure 29

[2] On the next 3 plots groups 3 and 4 appear in reverse order.

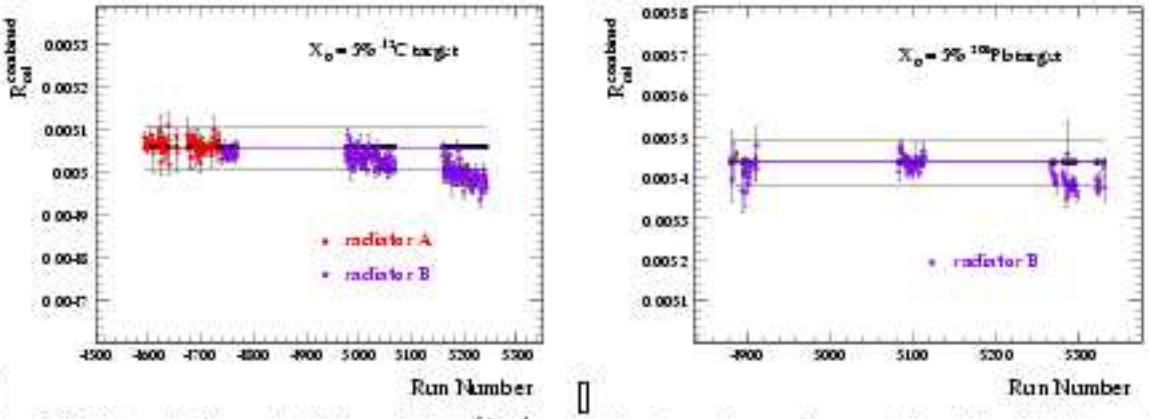

Figure 27: (a) Run dependence of [illegible] relative to pair ratio combined for 11 T-counters. (b) [illegible]

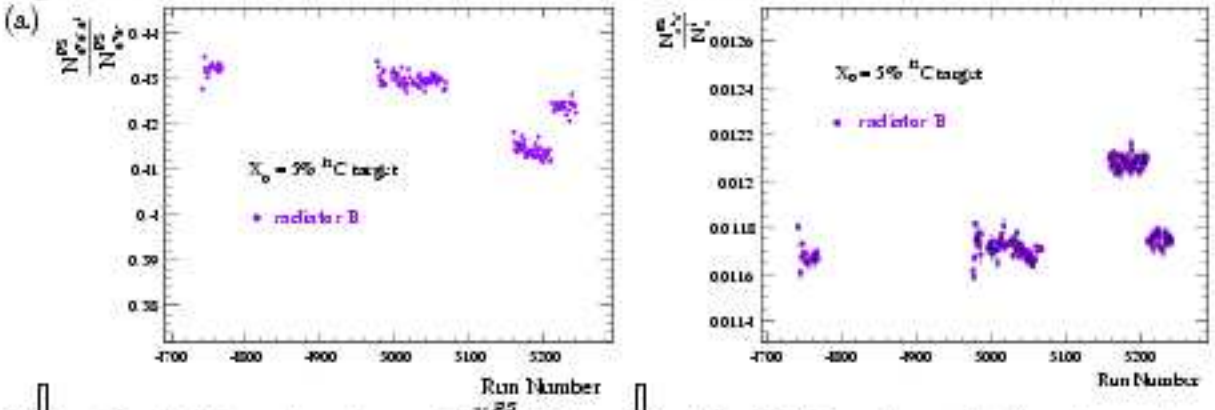

Figure 28: (a) Run dependence of $\frac{N^{PS}_{e^+e^-e^-}}{N^{PS}_{e^+e^-}}$ combined for 11 T-counters. (b) Run dependence of $\frac{N^{PS}_{e^+e^-}}{N^{T}_{e}}$ combined for 11 T-counters.

the drop in relative tagging ratios for group 4 is due to extra electrons rgistered in the tagger which have nothing in common with tagged photons on our target. The overall drop in $\frac{N^{PS}_{e^+e^-e^-}}{N^{PS}_{e^+e^-}}$ quantity can be explained by a drop in the absolute efficiency (hardware and reconstruction) of the tagging counters with increase of the beam intensity.

On Figure 31 I have plotted the the ratio of number of e^+e^- pairs registered in Pair Spectrometer to the number of electrons registered in the tagger. The plot shows $\sim 3.16\%$ raise when going from group 2 to group 3, which again could be explained by inefficiency of the tagger at high beam intensities.

5.3.13 Correction of Photon Flux for Affected Runs

Figure 27 part (a) shows that groups 4 and 3 of runs with ^{12}C target were influenced by extra electrons in the tagger. The qualitative study presented in Sections 5.3.11 and 5.3.12 indicates that those electrons do not create bremsstrahlung photons on our target. Hence, we need to correct the number of electrons in tagger when calculating the photon flux for affected runs.

For carbon target runs, the nominal values of the relative tagging ratios were obtained by calculating the weighted average for each of 11 T-counters.

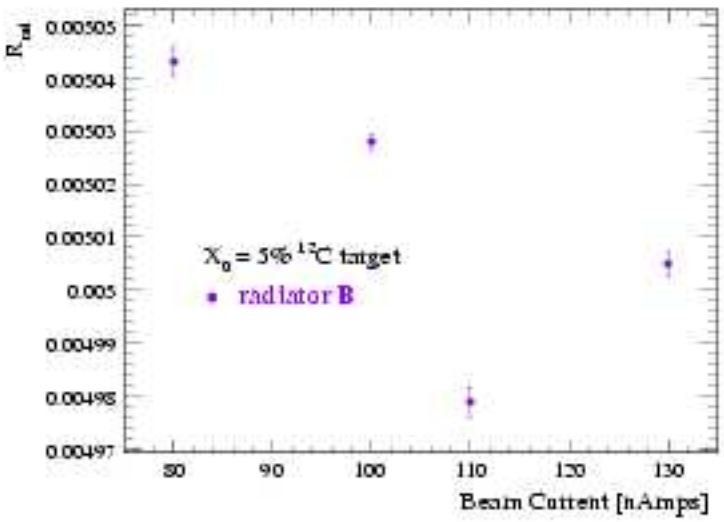

Figure 29: $R_{relative}$ vs. beam current, combined for 11 T-counters and averaged for all runs with same current. The drop in relative tagging ratios reflects the change in number of electrons in the Tagger.

From Figure 27 part (b) one can see that there are 3 distinct running periods for lead target. Let us call runs numbered 4950 and less group 1, runs numbered from 5070 to 5155 group 2 and runs numbered 5250 and up group 3. Using the same method as described above for runs with carbon target and information from group 2 one can obtain nominal values of relative tagging ratios for lead target runs (see Table ??). And based on these nominal values one can calculate correction factors for group 1 and group 3 of lead target runs (see Table ??).

5.4 A high precision measurement of the absolute cross section for pair production

The PrimEx experimental setup provides a unique opportunity to verify the luminosity normalization procedure (including both photon flux and target thickness) by measuring the absolute cross-section for a well known electromagnetic process, namely (e^+ e^-) pair-production, without any additional hardware development.

Cross-section calculations for the photo-production of e^+e^- – pairs on $^{12}_{6}C$ at photon energies of few GeV and small momentum transfer $|\vec{Q}| \sim 10keV$ relevant for the PrimEx experiment were provided by A. Korchin[3][?]. A summary of different contributions included in the cross-section calculation are listed below in decreasing order of significance:

- Bethe-Heitler mechanism for pair production on the nucleus. Two models, Thomas-Fermi-Moliere and Hartree-Fock, for the atomic form factor describing charge dis-

[3]A. Korchin, Kharkov Institute of Physics and Technology, Kharkov 61108, Ukraine.

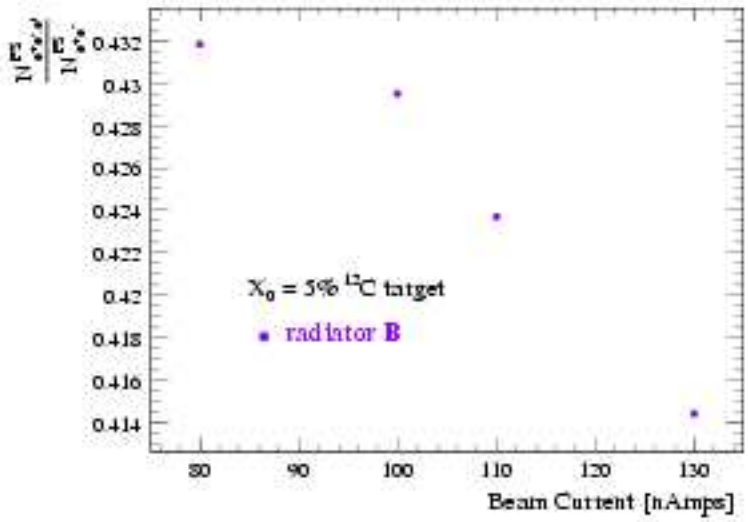

Figure 30: $\frac{N^{PS}_{e^+e^-e^-}}{N^{PS}_{e^+e^-}}$ vs. beam current, combined for 11 T-counters and averaged for all runs with same current, reflecting the loss of absolute efficiency of the Tagger.

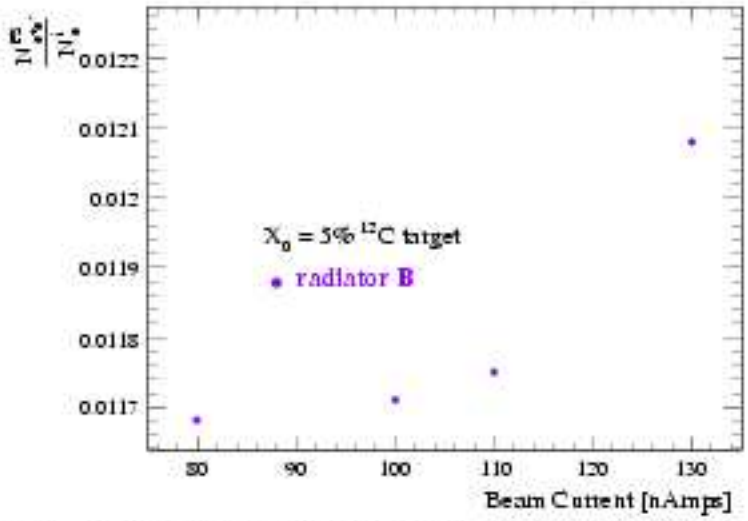

Figure 31: e^+e^-/e^- vs. beam current, combined for 11 T-counters and averaged for all runs with same current, reflecting the loss of absolute efficiency of the Tagger.

tribution of electrons were considered to account for screening effects due to atomic electrons. The Coulomb distortion effects have been included according to work of Bethe and Maximon (contribution to the e^+e^- cross-section of $\sim 80\%$).

- Pair production on atomic electrons taking into account the excitation of all atomic states and correlation effects due to precense of other electrons and the nucleus (contribution of $\sim 20\%$).

- QED radiative corrections (of order α/π with respect to the dominant contributions): (i) virtual-photon loops and (ii) real-photon process $\gamma + A \rightarrow e^+ + e^- + A + \gamma'$, (contribution of $\sim 1 - 2\%$).

- Nuclear incoherent contribution – quasi-elastic, or quasi-free process on the proton $\gamma + p \rightarrow e^+ + e^- + A + p$ (contribution of $< 0.05\%$).

- Nuclear coherent contribution, *i.e.* virtual Compton Scattering, a two-step process $\gamma + A \rightarrow \gamma^* + A \rightarrow e^+ + e^- + A$ (contribution of $\sim 10^{-5}\%$).

As an example, the Figure 32 shows the calculated energy distribution of electrons produced by $5.46 GeV$ photons on $^{12}_{6}C$ target. The calculations based on three different models of atomic form factors are shown: Hartree-Fock (HF), Thomas-Fermi-Moliere (TFM) and a simpler monopole approximation introduced by Tsai. As one can see on the figure the cross-section slightly decreases compared to TFM if HF from factor is used. The difference between the cross-section based on Hartree-Fock atomic form factor and the one based on Thomas-Fermi-Moliere model is of the order of $< 1\%$ which demonstrates accuracy of the calculations.

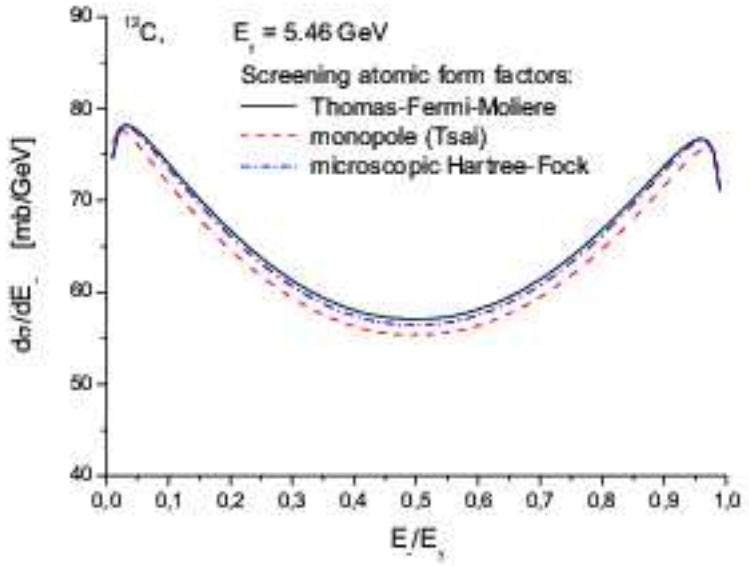

Figure 32: Calculated energy spectrum of electrons in pair-production on $^{12}_{6}C$ for $5.46 GeV$ photons.

A schematic of a pair-production event as seen by the PrimEx experimental setup (upstream of the tagger) is shown on Figure 33:

For pair-production cross-section measurement, both the incident photon energy and timing information were determined by the tagger. The strength of the magnetic field of the PS dipole was lowered (to ~ 0.220 and $0.293\ Tesla \times m$) and the electron-positron pairs were swept into the calorimeter where the energy and position of the each particle was measured. The trigger signal, a coincidence between Tagger MOR and HyCal, recorded in a TDC provides timing information of the $e^+\ e^-$ - pair (see Figure ??).

Following the event selection recipe introduced in Section ?? one can obtain the spectrum of selected photons which is shown on Figure 34.

The even E-channels are the product of overlapping nature of physical E-counters and have smaller width compared to odd E-channels which results in an uneven population of various E-channels. The level of occupancy of an E-channel also depends on it's geometrical correspondence to odd or even T-channel.

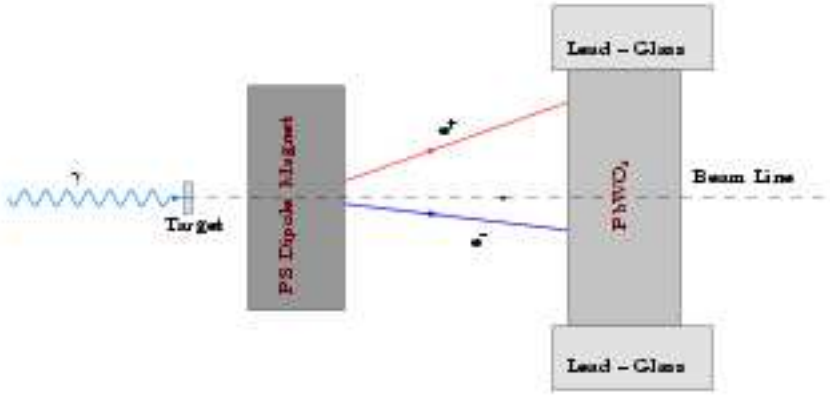

Figure 33: Schematics of a pair-production event as seen by PrimEx experimental setup (top view)..

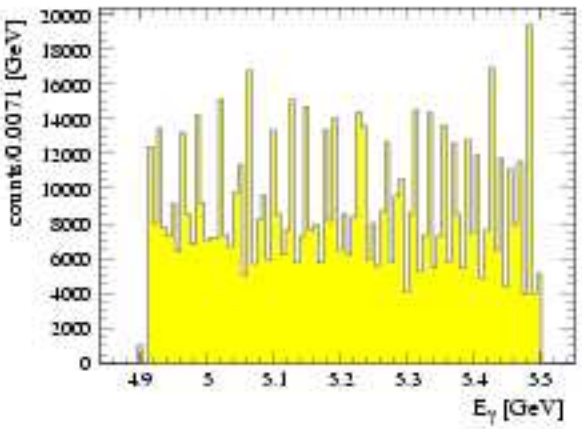

Figure 34: Spectrum of incident photons showing almost uniform distribution of gammas over the tagged energy range ($4.874 - 5.494 GeV$).

The energy range represented on Figure 34 corresponds to 114 E-channels. The E-channels are grouped by 11 or 12 to comprise 10 energy sub-ranges providing finer photon energy binning. The boundaries of these 10 energy ranges are determined by average energy of the first and last E-channel in the respective sub-range.

The $\pm 15ns$ timing cut introduced in Section ?? for event selection can be further refined by examining the Tagger-HyCal time differences, *i.e.* "tdiff"-spectra, for individual T-channels (see Figure 35).

On parts (a) and (b) of Figure 35, showing the "tdiff" spectra for T-channels #3 and #12 respectively, one can see that the mean value and the standard deviations are different for the spectra of different T-channels. Figure 35 also shows a tail trailing on the positive side of the spectrum. A conservative, asymmetric cut $(-5\sigma, +8\sigma)$ about the mean value has been applied to the "tdiff" distribution of each T-channel to account for these effects.

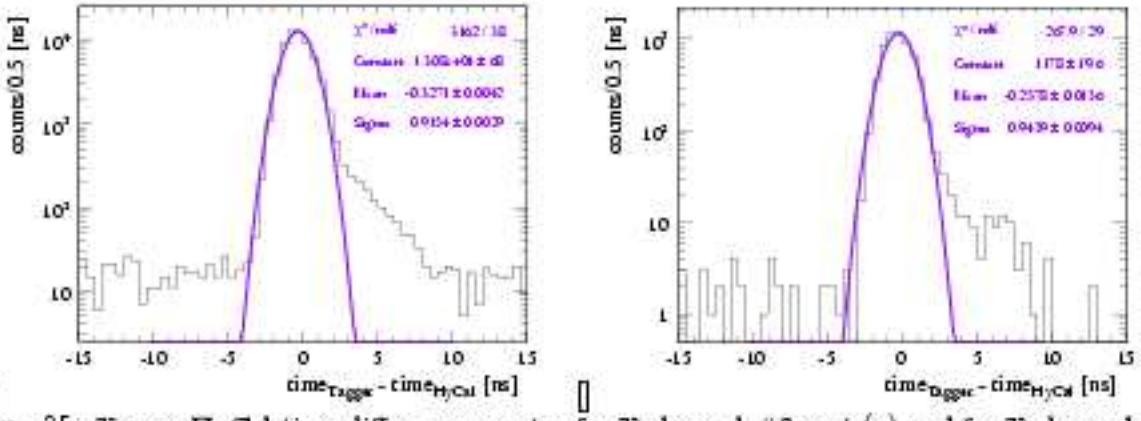

Figure 35: Tagger-HyCal time difference spectra for T-channel #3 part (a) and for T-channel #12 (b). As a sample, Figure 36 shows distribution of X and Y coordinates and the energy position correlation for events with incident photon energy in the range $5.145 - 5.201 GeV$, *i.e.* energy bin 5 after the timing cut of $(-5\sigma, +8\sigma)$. The negative X coordinates correspond to positrons and the positive X coordinates represent electrons.

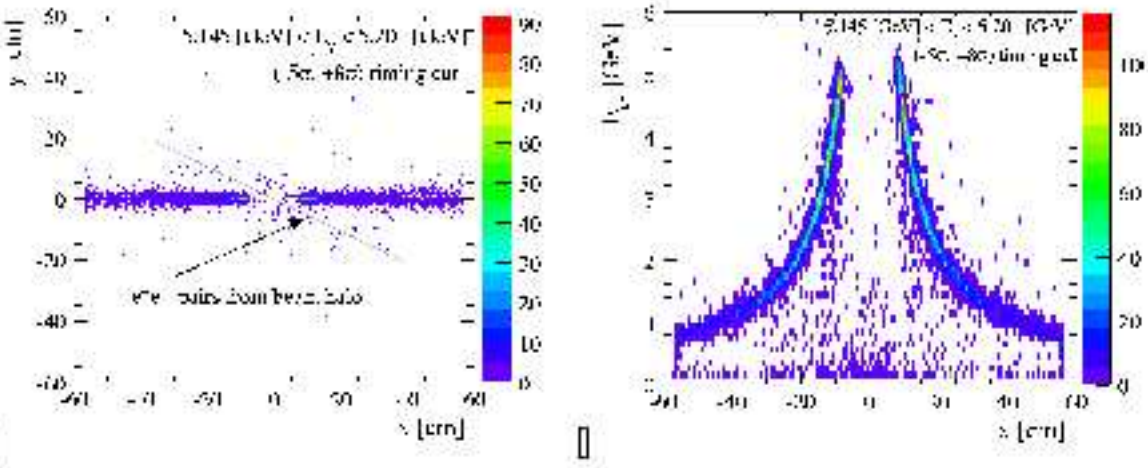

Figure 36: (a) Distribution of X and Y coordinates of clusters reconstructed in HyCal. (b) Correlation of energy and deflection in the magnetic field for clusters reconstructed in HyCal.

One thing to note for future reference is the fact that in contrast to *GEANT4* simulation, where the electrons and positrons have identical energy spectrum (see Figures ?? and ??), in the data electrons have higher end point energy compared to positrons (see Figure 36).

On part (a) of Figure 36 one can see a ring of "Compton" photons around the central opening of the HyCal and a faint line with negative slope due to pair-production generated by the halo of the beam hitting the photon beam collimator upstream of the experimental target. The electrons and positrons created by the halo on the collimator are first deflected in the field of the permanent magnet in vertical direction and then by the Pair Spectrometer dipole magnet in horizontal direction creating the slopped line.

To eliminate the e^+e^--pairs created by beam halo and most of Compton photons a cut on the Y coordinate of particles is used. The distributions of Y coordinates for positrons and/or

electrons, shown on Figure 37, created by incident photons of energy $E_{\gamma\ bin1} = 4.90 - 4.96 GeV$ and $E_{\gamma\ bin10} = 5.45 - 5.49 GeV$ have nearly identical widths which allows for a single cut range ($|Y| < 5cm$) for all the energies of the photons. As shown by the simulation (see Figure ??) such cut would affect electrons/positrons created on the target if their energy is less than $\sim 1.6 - 1.7 GeV$.

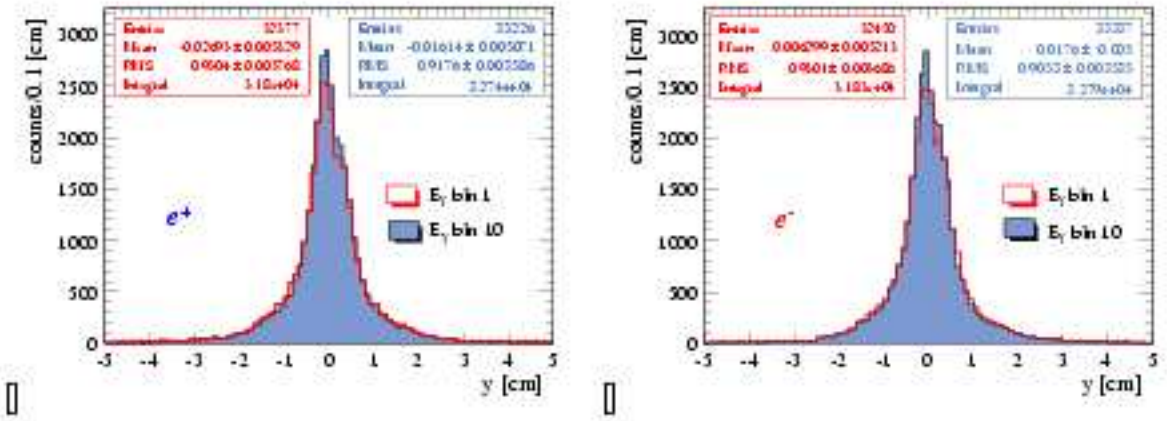

Figure 37: Distribution of Y coordinates of clusters reconstructed in HyCal due to incidnet photons of various energy: (a) positrons and (b) electrons.

As mentioned previously pair-production data was taken with various settings of Pair Spectrometer dipole (see Section ??). For the highest field setting of $\sim 0.293\ Tesla \times m$ momenta of $1.6 GeV$ and less correspond to deflections of particles in the field of the dipole of $\sim 37.17cm$ or more, *i.e* deflections into the outer Lead-Glass layer of the calorimeter. A cut of $E_{e^\pm} > 1.695 GeV$ on the energy of leptons limits the analysis to the inner, high resolution, Lead-Tungstate layer of the HyCal which extends out to $\pm 35.275cm$ and allows to compare data from runs with different field setting. Table ?? lists the pair-production data runs with the setting of the Pair Spectrometer dipole for each run the minimum lepton energy cut and the corresponding minimum deflection in horizontal direction.

As shown on part (a) of Figure ?? Compton electrons take most of the energy at the kinematic regime of the PrimEx experiment, thus a cut $E_{e^\pm} > 1.2 GeV$ would also eliminate a large amount ($\sim 59.9\%$) of Compton photons some of which would otherwise be reconstructed in Lead-Tungstate part of the calorimeter (see Figure 38). It is worth noting that the distributions of X and Y coordinates for Compton photons are identical due to azimuthal symmetry of Compton scattering.

The final step toward the yield extraction is the subtraction of the background due to Compton scattering under the electron arm. For this purpose the energy distribution of Compton electrons was generated for each photon energy bin as described in Section ?? (see Figure ??) and smeared with detector resolution function (see Figure ??). The resulting distribution, shown on Figure 39, is subtracted from data with appropriate scaling factor. The scaling factors, listed in Table ?? were determined according to the photon flux in each

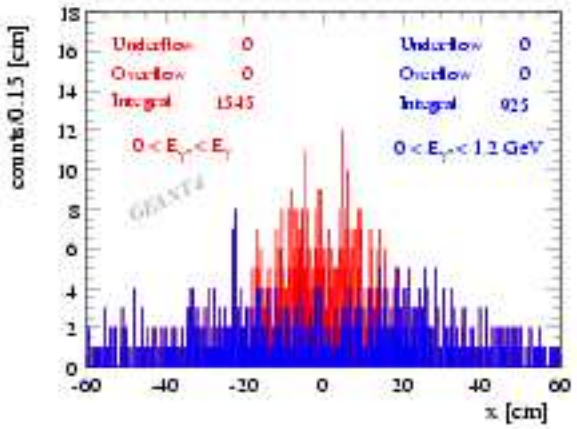

Figure 38: Distribution of X coordinates of scattered photons in simulated Compton events.

run keeping in mind that in total 2.5×10^7 photons were thrown to generate the Compton electron background. The photon flux for the pair-production runs is listed in Appendix ??.

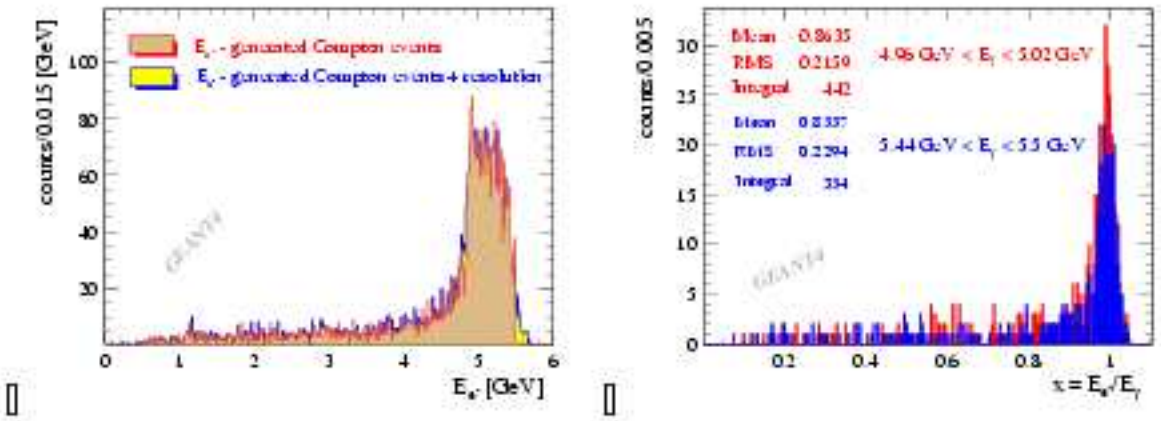

Figure 39: (a) Energy spectra of the Compton electrons generated in *GEANT4* simulation by incident photons in energy range $(4.874 - 5.494 GeV)$. The effect of detector resolution is shown by the blue histogram. (b) Energy distribution of Compton electrons for incident photon energy bins 2 and 10.

An example of the high energy part of the electron spectrum, which is most affected by the background, is shown on Figure 40 before and after subtraction of Compton background.

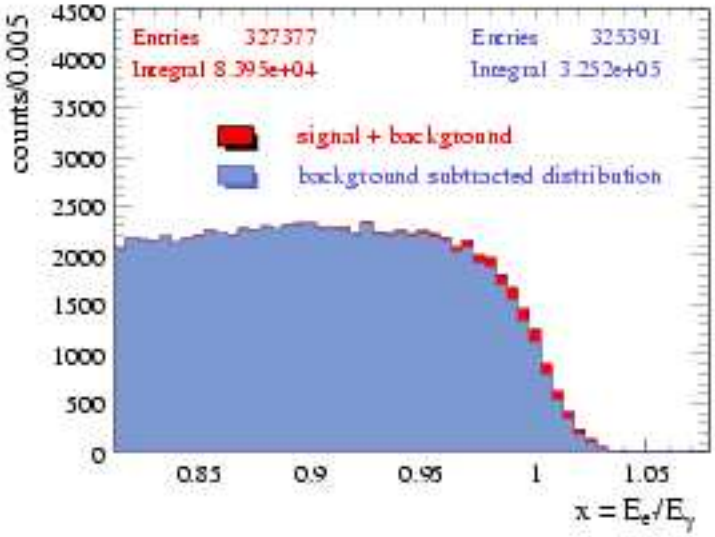

Figure 40: Energy spectrum of electrons before and after subtraction of Compton background.

As mentioned in Section ?? the number of atoms per unit area in Carbon target is: $0.1066 \times 10^{24}(\pm 0.053\%)$ $[\frac{1}{cm^2}]$. Knowing the photon flux one can easily convert yields, obtained as described in Section ??, into cross-sections. But before the cross-section obtained in the experiment can be compared to the one calculated by theory one needs to take into account the effects of HyCal resolution and the energy losses of electrons and positrons before they reach the calorimeter due to secondary interactions in the target and the helium before they reach the calorimeter (see Figure 41). To do so the *GEANT4* has been utilized.

First a photon energy is picked according to the spectrum of photons present in the data (see Figure 34). Then an electron is generated with a fraction of photon energy according to the spectrum shown on Figure ?? part (b) and with coordinates $(0.,0.,Z)$ where the Z-coordinate is picked based on the distribution of Z-positions of vertexes of e^+e^- events generated in the first stage of the simulation (see Figure ??). In total 10-million such events were generated and tracked through the *GEANT4* setup introduced in Section ?? recording the energies of the particles at the surface of the calorimeter. The energies of the electrons, recorded in simulation at the surface of the calorimeter, are smeared according to resolution function of the calorimeter shown on Figure ??. The generated yields were normalized to obtain a differential cross-section according to the calculated total cross-section for $E_\gamma = 5.18 GeV$ (see Table 1).

For electrons the *GEANT4* allows for multiple scattering, ionization and bremsstrahlung providing cross-section accuracy for these processes of $\sim 5-10\%$ [?]. Let us define $\sigma_0 = \frac{d\sigma_0}{dx}$ to be the calculated cross-section for pair production and $\sigma_1 = \frac{d\sigma_1}{dx}$ to be the differential cross-section convoluted with the energy losses and the detector resolution then $r = 100\frac{\sigma_0-\sigma_1}{\sigma_0}$ will be the percent deviation of the differential crossection convoluted with the energy losses and detector resolution from the calculated value. On Figure 42 the r is ploted as a function of the fraction of energy of the incident photon taken by the electron.

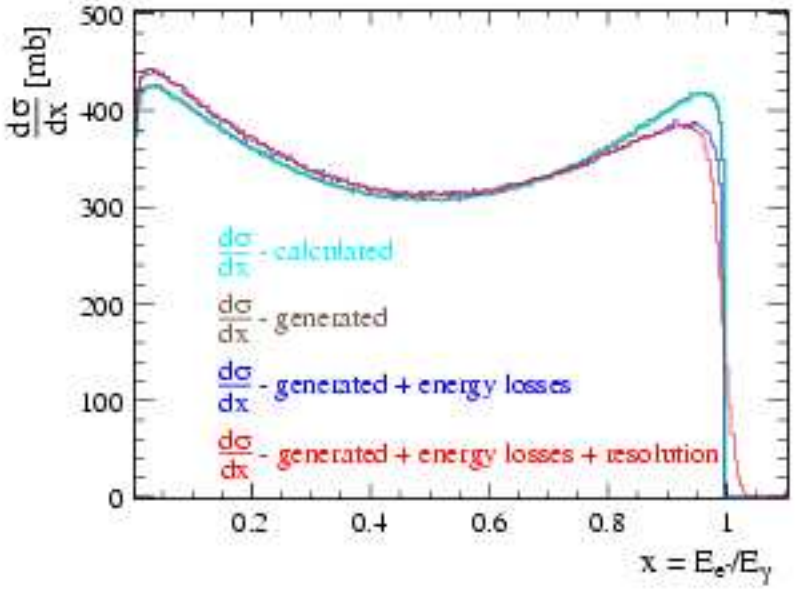

Figure 41: Absolute cross-section for pair-production differential in fraction of energy of photon taken by the electron for $E_\gamma = 4.91 - 5.46 GeV$. The effect of energy losses in the target and the helium "buffer" is also shown as blue histogram.

Table 1: Total cross-section for pair-production calculated for the central values of the 10 energy bins.

Energy bin ID	E_γ avg. GeV	$\sigma^{e^+e^-}_{total}$ mb
1	4.91	351.106
2	4.97	351.176
3	5.03	351.244
4	5.11	351.328
5	5.18	351.408
6	5.23	351.461
7	5.28	351.513
8	5.34	351.574
9	5.41	351.644
10	5.46	351.692

One can see that, for electrons or positrons with energy fraction $0.9 < x < 1.0$ the percent difference between calculated cross-section and one modified by energy losses and detector resolution is changing rapidly ($5\% < r < 50\%$). Hence, for this region of x one could expect up to $2 - 5\%$ descrepancy between experimental cross-sections and theory (modified by energy losses and resolution) due to the uncertainty of the *GEANT4* calculation of the energy losses (see Figure 43). To minimize the potential systematic errors it is preferable to

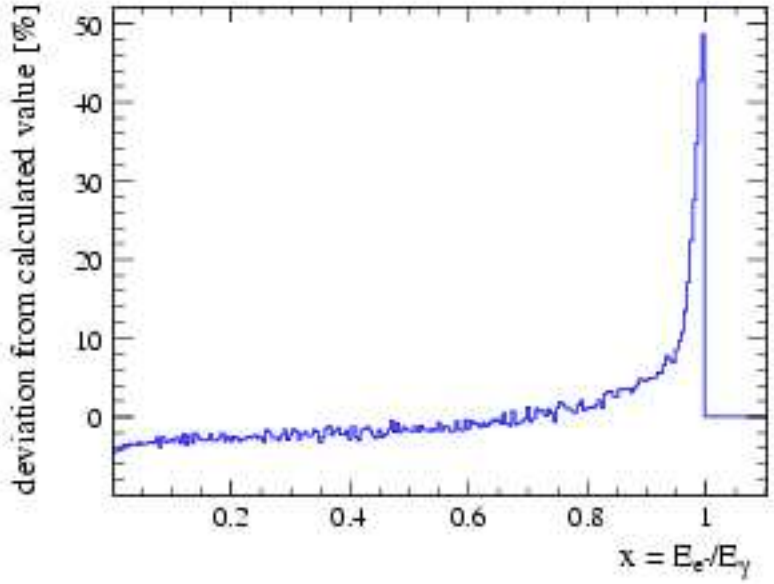

Figure 42: Percent deviation of the differential cross-section convoluted with energy losses and detector resolution from the calculated value.

compare the experiment and theory for $0.3 < x < 0.85$ where the effect of the energy losses on the cross-section is less than 5%.

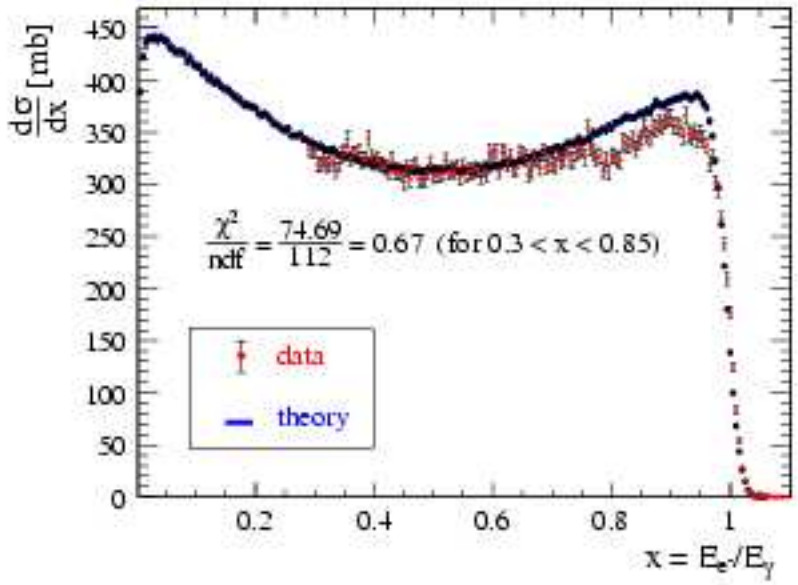

Figure 43: Differential cross-section for e^+e^--production extracted on electron arm.

Table 2 lists the theoretical and experimental pair production cross-sections for various runs integrated between x_{min} and x_{max}. Where x is the fraction of energy of the incident photon taken by the electron ($x = E_{e^-}/E_\gamma$).

Table 2: Pair production cross-section integrated between x_{min} and x_{max}.

Run Number	x_{min}	x_{max}	$\sigma_{experiment}[mb]$	$\sigma_{theory}[mb]$	$(1-\sigma_{experiment}/\sigma_{theory})[\%]$
5142	0.3	0.85	181.897	185.754	2.10
5314	0.3	0.85	188.568	185.754	−1.52
5142	0.4	0.85	149.311	152.7	2.22
5314	0.4	0.85	154.711	152.7	−1.32
5141	0.4	0.85	152.281	152.7	0.27

- Yield Statistics.

Table 3: Statistical error for the e^+e^- yields extracted between x_{min} and x_{max}.

Run Number	x_{min}	x_{max}	dY [%]
5142	0.3	0.85	0.21
5314	0.3	0.85	0.24
5142	0.4	0.85	0.23
5314	0.4	0.85	0.27
5141	0.4	0.85	0.27

- Number of carbon atoms per unit area – (0.05%).

  The number of atoms per unit area - n is given by:

$$n = \frac{N_{atoms}}{A} = \frac{\rho \ell}{m} \tag{7}$$

  where A is the cross-section of the beam, ρ is the density of the target material, ℓ is the target thickness and m is the mass of the atom of the target material. For the carbon taget of PrimEx experiment one has $\ell = 0.966cm(\pm 0.039\%)$ and $\rho = 2.198g/cm^3(\pm 0.014\%)$ [?]. Thus for the carbon target the number of atoms per unit area is $n_{C^{12}} = 1.066 \times 10^{23} cm^{-2}(\pm 0.053\%)$.

- Photon Flux.

  For details on error evaluation procedure for photon flux see Sections ?? and ??. The systematic error in photon flux determination, arising from the systematic uncertainty in the measuerement of the absolute tagging ratios and the uncertainty in electron counting due to beam intensity variations, is 0.97%.

The statistical error on the photon flux, in pair-production data, has a small contribution (0.06%) from error on absolute tagging ratios and is dominated by the electron counting statistics. The combination of both is given in Table 4:

Table 4: Statistical error on the number of photons for pair-production runs.

Run Number	N_γ	dN_γ[%]
5142	1.19797e+07	0.34
5314	8.62907e+06	0.40
5141	8.59525e+06	0.40

- Background subtraction.

  As previously discussed the background from Compton electrons is significant in the region of $x = E_{e^-}/E_\gamma > 0.9$ (see Figure 40). Figure 44 shows that the relative contribution of the Compton electrons under electron arm for $0.3 < x < 0.85$ is not larger than 0.3%. Hence, a conservative 50% error in determination of the Compton electron background, due to low statistics of generated events, results in 0.15% or lesser error on the pair-production cross-section.

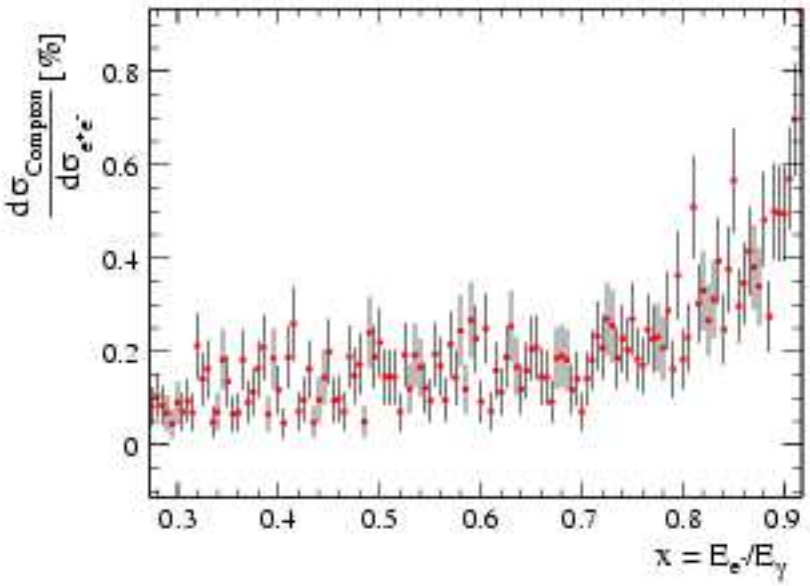

Figure 44: Ratio of Compton and pair-production yields for $0.3 < x < 0.85$.

The background due to Compton photons in region $0.3 < x < 0.85$ is completely eliminated by cuts: $E_{lepton} > 1.2GeV$ and $|Y_{lepton}| < 5cm$.

- HyCal Resolution.

  To study the effect of the HyCal resolution the *GEANT4* simmulation was used. The integrated cross-section for pair-production was calculated for $0.3 < x < 0.85$ while

smearing the energy of the particles with a gaussian. The width of the gaussian has been varied between 0.016 and 0.03 in increments of 0.002 to mimic the resolution of the calorimeter $(1.6 - 3.0\%)$. As one see from Table 5 the effect of the detector resolution on the cross-section is less than 0.12%.

Table 5: Effect of detector resolution on e^+e^- cross-section integrated between $x_{min} = 0.3$ and $x_{max} = 0.85$.

Smearing parameter [%]	σ [mb]
1.6	185.746
1.8	185.788
2.0	185.856
2.2	185.833
2.4	185.828
2.6	185.841
2.8	185.957
2.6	185.896

- Multi-photon events (see Section ??).

  The cross-section calculation was repeated for run #5142 accepting only events with 1 photon reconstructed in the tagger. The photon flux was recalculated ($N_\gamma = 230001$ and $dN_\gamma = 0.54\%$). The procedure resulted in e^+e^- cross-section of 182.014 [mb] for $x_{min} = 0.3$ and $x_{max} = 0.85$ with a statistical error on the yield of (0.35%). The obtained cross-section is in prfect agreement (within the statistical errors) with the value listed in Table 2. However, to be c onservative one can assume an error of 0.06% due to photon reconstruction ambiguity.

- HyCal calibration.

  If one assumes that all other effects have been accounted for or they are constant over time, the error on the cross-section, due to drifting detector gains, can be inferred by comparing the cross-sections from various runs integrated between same values of x_{min} and x_{max} (see Table 2). Assuming independent errors, for error due to detector calibration (plus all other time dependent systematic effects) one has an upper limit of 1.92%.

  Table 6 summarizes the error on the experimental cross-sections listed in Table 2.

- Error on the theoretical cross-section.

  As already mentioned in Section ?? the error on the theoretical value of the cross-section due to the choice of the atomic screening form factor is on the order of $\sim 1\%$.

  The experiment is being compared to a theoretical cross-section convoluted with energy losses in the target. The *GEANT4* provides an accuracy of $5 - 10\%$. To evaluate the effect of this error on convoluted theory the energy losses in simmulation were

Table 6: Summary of errors.

	Effect	Error (%)
Statistical	Yield statistics	run dependent (~ 0.25)
	Photon flux ($R_{absolute}$ and electron counting)	run dependent (~ 0.37)
Systematical	Photon flux ($R_{absolute}$ and electron counting)	0.97
	Number of Carbon atoms in the target	0.05
	Background subtraction	0.15
	HyCal resolution	0.12
	Photon misidentification/double counting	0.06
	HyCal calibration	< 1.92
Total		$\sim \pm 0.44(stat.) \pm 2.16(sys.)$

artificially varied by $\pm 10\%$ and the theoretical cross-section was recalculated for region $0.3 < x < 0.85$ resulting in $\sim 0.32\%$ difference.

Thus the estimated uncertainty on the theory convoluted with energy losses in the traget is 1.05%.

Given the above consideratons the experimentaly obtained cross-section, for $0.3 < x < 0.85$ is in remarkable agreement with theory.

5.5 Absolute cross section for electron Compton scattering

5.6 Photon beam position monitor

A photon beam position detector was constructed by the collaboration that had provided continuous real time photon beam position and profile information during the first experiment, as well as information in the data stream for off-line data analysis. This detector consists of two identical modules crossed at right angles to each Other(shown in 45 to give the beam profile along both x and y directions. Each module is a linear hodoscope of multichannel Bicron scintillating fibers (X module has 61 channels and Y module has 62) forming a plane perpendicular to the photon beam. This detector is mounted on a remote controlled table with the X and Y motion placed just the HYCAL at nominal beam path. Each scintillating fiber has dimension of $2 \times 2 \times 13$ mm^3. The scintillating light from the fibers transmit through the light guide and is detected by four 16-channel R5600-M16 Hamamatsu PMTs. A compact electronics module provides 64 channels of amplifier and discriminators for anode signals, then convert them to ECL readout through a time-over-threshold circuit. The ECL signals are sent over to SIS3801-256-flat scalars and read into epics systems. During the run, the x and y beam profiles were displayed through a GUI for on-line beam control (shown in

figure ??) and read into DAQ for off-line analysis. This device performed beautifully during the experiment and provided an excellent beam diagnosis tool.

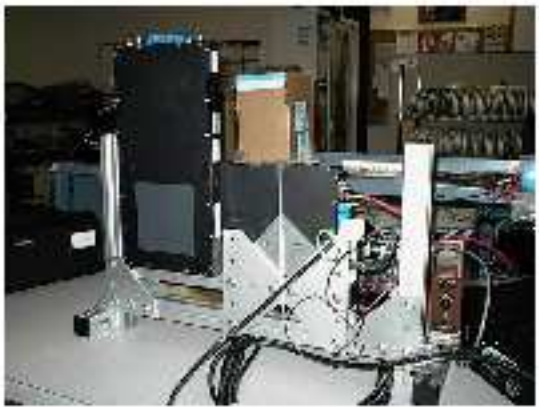

Figure 45: The PrimEx photon beam position detector.

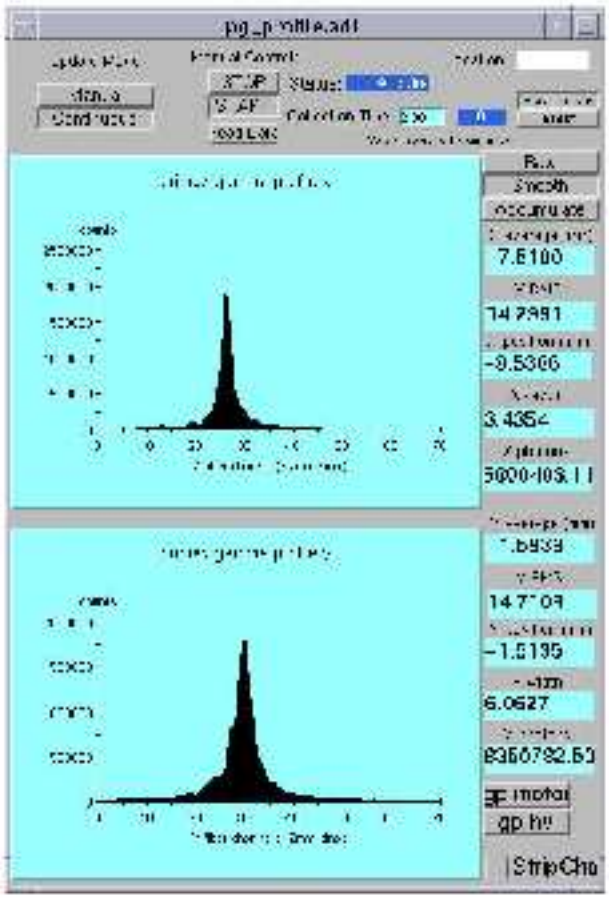

Figure 46: Photon beam position on-line display.

5.7 Data Acqusition and electronics

6 Plans for a future run

6.1 New improvements

6.2 Run time and schedule

7 Summary

8 Appendix I: Previous Experiments

8.0.1 The direct method

A direct measurement of the π^o lifetime can be made by observation of the decay distance between the production and decay points. This has proven difficult because of the high spatial resolution which is required due to the short lifetime, $\tau \simeq 10^{-16}$ sec. To be able to discern distinct production and decay points, one must take advantage of relativistic time dilation to have the pion survive long enough in the laboratory frame. Additionally, good knowledge of the energy distribution of the produced pions is necessary in order to extract the lifetime via this method.

The most recent result employed direct method was carried out at the CERN SPS in 1985 (shown in figure ??). In this experiment, a 450 GeV/c proton impinged upon two tungsten foils whose separation was variable. The first foil served as the π^o production target, and the second foil converted the π^o decay photons to electron-positron pairs, and the positrons were subsequently detected. By measuring the positron rates for three different foil spacings ranging from 5 to 250μm, the authors were able to determine the lifetime. The dominant systematic errors arise from uncertainties in the π^o spectrum which was not measured but was assumed to be the arithmetic mean of the π^+ and π^- spectra. In addition, corrections had to be made for the Dalitz decay of the π^o's, conversion of the photons in the π^o production target, prompt positron and photon production, and positrons from the decay of η's. A pion lifetime of $\tau_{\pi^o} = (0.897 \pm 0.022 \pm 0.017) \times 10^{-16}$ seconds was reported[?], corresponding to a width of $\Gamma_{\pi^o} = (7.34 \pm 0.18 \pm 0.11)$ eV.

It is interesting to note that this experiment, the most precise of those performed to date, gives a result which is smaller than the leading order chiral anomaly prediction[?, ?]. Furthermore, with the latest calculations based on both next-to-leading order chiral theory and QCD sum roles described above, the discrepancy between this measurement and theory widens to more than three standard deviations. The experiment proposed here will directly address this discrepancy.

8.0.2 Measurements using $\gamma\gamma$ collisions

The π^o width has been measured using electron-positron collisions at DESY via $e^+e^- \rightarrow e^+e^-\gamma^*\gamma^* \rightarrow e^+e^-\pi^o \rightarrow e^+e^-\gamma\gamma$ [?]. The incident leptons are scattered at very small angles and are not detected in the final state. In so doing, they radiate quasi-real photons that

couple to the π^o which is subsequently identified in an invariant $\gamma\gamma$ mass spectrum. The photons were detected using the Crystal Ball detector which consists of a large array of NaI(Tl) crystals providing 93% solid angle coverage. Contributions to the systematic error included luminosity normalization, detector efficiencies, cosmic ray rejection, and beam-gas collisions. The latter effect arises from the production of π^o's via the interaction of the leptons with the residual gas in the beam pipe. The resulting width obtained was $\Gamma_{\pi^o} = (7.7 \pm 0.5 \pm 0.5)$ eV, very close to the prediction of the anomaly but with a relatively large error. The value obtained in this experiment is the same as the Particle Data Book average but was not included in this average[?].

8.0.3 Measurements using the **Primakoff** effect

The Primakoff effect, *i.e.* photopion production from the Coulomb field of a nucleus[?], has been used in a number of experiments to study the π^o lifetime [?, ?, ?, ?]. The production of π^o's in the Coulomb field of a nucleus by real photons is essentially the inverse of the decay $\pi^o \rightarrow \gamma\gamma$, and the cross section for this process thus provides a measure of the π^o lifetime.

Using bremsstrahlung beams of energy 4.4 GeV and 6.6 GeV at Cornell, Browman *et al.*[?] measured the Primakoff cross sections on several nuclei, and obtained a total decay width of $\Gamma_{\pi^o} = (8.02 \pm 0.42)$ eV. However, as was pointed out in [?, ?] the quoted error, does not have any contribution from uncertainties in the luminosity or detection efficiency (see table 1 of [?]), and is an underestimate. An analogous measurement of the η width[?] using the Primakoff effect employing a very similar setup and analysis procedure is not in agreement with other experiments.

The other two Primakoff measurements shown in figure ?? were performed with bremsstrahlung beams of 1.5 and 2.0 GeV at DESY[?] and 1.1 GeV at Tomsk[?]. From figure ?? it can be seen that the DESY measurement is high compared to the theoretical prediction and the Particle Data Book average. Although both of these measurements have relatively large errors they were included in the Particle Data Book average[?]. An older Primakoff experiment performed with 0.95 and 1.0 GeV bremsstrahlung beams at Frascati[?] has not been included in the Particle Data Book average and is not shown in figure ??.

In view of the strong interest in the subject, the dispersion of the previous results, and the recent availability of high intensity, high energy tagged photon beams, a high precision, state-of-the-art measurement of the π^o lifetime is needed. In past several years, PrimEx collaboration has developed an experimental setup combining existing Hall B tagged photon facility at TJNAF with a newly developed a state-of-the-art, high resolution electromagnetic colorimeter. It will enable a measurement which will offer three distinct advantages over previous measurements involving bremsstrahlung beams: (1) the quasi-monochromatic nature of the tagged beam will enable a clean kinematical separation of the Primakoff mechanism from various background processes, (2) the tagging technique will enable significantly better control of systematic errors associated with the photon flux normalization, and (3) high resolution and high efficiency electromagnetic calorimeter will enable precise measurements on the invariance mass and production angle of the π^0's. The first PrimEx experimental data set was collected in Hall B in fall 2004. The preliminary result is $\Gamma(\pi^0 \rightarrow \gamma\gamma) = 7.93 + -2.1\%(stat) + -2.0\%(sys)$ eV. More beam time is requested in this proposal to reach our final goal of $\sim 1.4\%$ precision.